Research Article **Open Access**

Erasmo Viola*, Marco Miniaci, Nicholas Fantuzzi, and Alessandro Marzani

Vibration analysis of multi-stepped and multi-damaged parabolic arches using GDQ

Abstract: This paper investigates the in-plane free vibrations of multi-stepped and multi-damaged parabolic arches, for various boundary conditions. The axial extension, transverse shear deformation and rotatory inertia effects are taken into account. The constitutive equations relating the stress resultants to the corresponding deformation components refer to an isotropic and linear elastic material.

Starting from the kinematic hypothesis for the in-plane displacement of the shear-deformable arch, the equations of motion are deduced by using Hamilton's principle. Natural frequencies and mode shapes are computed using the Generalized Differential Quadrature (GDQ) method. The variable radius of curvature along the axis of the parabolic arch requires, compared to the circular arch, a more complex formulation and numerical implementation of the motion equations as well as the external and internal boundary conditions. Each damage is modelled as a combination of one rotational and two translational elastic springs.

A parametric study is performed to illustrate the influence of the damage parameters on the natural frequencies of parabolic arches for different boundary conditions and cross-sections with localized damage. Results for the circular arch, derived from the proposed parabolic model with the derivatives of some parameters set to zero, agree well with those published over the past years.

Keywords: Parabolic Arches; Generalized Differential Quadrature Method; Damage; Numerical Methods

DOI 10.1515/cls-2015-0003
Received September 25, 2014; accepted November 18, 2014

***Corresponding Author: Erasmo Viola:** Department of Civil, Chemical, Environmental and Materials Engineering - DICAM, University of Bologna, Viale del Risorgimento 2, 40136, Bologna, Italy, E-mail: erasmo.viola@unibo.it, tel. +39 051 2093510

Marco Miniaci, Nicholas Fantuzzi, Alessandro Marzani: Department of Civil, Environmental and Materials Engineering - DICAM, University of Bologna, Viale del Risorgimento 2, 40136, Bologna, Italy

1 Introduction

Curved beams represent fundamental components of many engineering structures such as bridges, roofs, vaults, underground galleries, etc. Therefore, the study of their static and dynamic behaviour has attracted considerable attention in the scientific community. Nowadays, investigations on this subject involve both theoretical formulations [1–3] and practical applications [4–8].

Many researchers have approached the issue through numerical methods, which were mainly based on finite elements, Rayleigh-Ritz, Galerkin, and cell discretization, see [9–15], among others. In this work theoretical and numerical approaches are given.

In order to obtain a computationally efficient and accurate solution for the free vibration of multi-stepped and multi-damaged parabolic arches, a Generalized Differential Quadrature (GDQ) formulation has been developed. The present numerical approach is well known in literature for its high accuracy, stability and reliability. For further details on this subject the interested reader is referred to [16–19]. The analysis of curved beams has been a subject of considerable research interest over the years. However, to the best of the authors' knowledge, very few researchers have investigated damaged parabolic arch structures, one of them being [20]. The majority of the cited works are limited to circular arches, despite of the wide diffusion of parabolic structures in civil engineering practice. Furthermore, most of the studies on vibration analysis of damaged arches have been confined to structures having only one notch.

Since the aim of this work is to extend the results found out in [21] for circular arches, free in-plane vibrations of undamaged and multi-damaged parabolic arches are studied. In both cases, the stepped parabolic arch is divided into a number of arches with constant cross-sections. For the damaged arch, elastic hinges at the notched sections are also introduced. Consolidated structural software (such as ABAQUS and Straus7) was used to validate the in-house formulation.

The governing equations of the arches include fourth and second order partial differential equations (PDEs), for-

mulated for the first time both in standard and mixed variational forms in [22].

Herein, starting from the kinematic hypothesis for the in-plane displacement of the shear-deformable arch, the equations of motion are deduced by using the Hamilton principle. Afterwards, the influence of notches on the formulation is investigated, starting from the well-known concept that damage in a structure introduces local flexibility.

The notch is modelled as three massless elastic springs, the damage being located at the cross-section level. Each spring connecting two arch portions is supposed to have axial, normal and rotational elastic stiffness that allow discontinuity in the axial and transversal directions, as for rotation. These generalized displacements are proportional to the axial and shear forces as well as the bending moment in the structure, respectively. Interaction between the springs is neglected in this first approach, even though more complex elastic hinges have been also used in vibrating problems involving structural elements, see [23] among others.

Each notch divides the structure into two adjacent elements. The differential equations of motion are established for each segment of the parabolic arch. After imposing boundary conditions and compatibility conditions at the notched cross-sections of the arch, the solution of the investigated problem can be derived.

The solution procedure for the fundamental system of equations starts from the strong formulation of the problem. The numerical method is focused on the GDQ method and Generalized Differential Quadrature Element (GDQE) techniques. The GDQ method is an extension of the original Differential Quadrature (DQ) method introduced in [24, 25]. This procedure was followed and extended in [26–32]. Some researches coupled a method applicable to single domains with finite element methods. The GDQ method was developed in [33]. Due to the extremely simple mathematical formulation of the technique, several papers [34–37] followed. Other papers about domain decomposition and GDQ were published recently [38–40].

It is worth mentioning that the effect of cracked beams on the dynamic behavior of beams and like structures has been investigated by a number of authors [41–44]. In all the above structures the cracks are always considered open and the crack does not propagate during vibration. In the analyses in [45, 46], the cracks are also considered open. Numerical modelling for evaluating the stress intensity factors have been proposed, for instance, in [47, 48].

Moreover, dynamic non-destructive damage detection methodologies have been proposed for straight beams [49, 50], curved beams [51], plates [52] and for truss structures [53], among others.

Following the introduction above, a brief review of the GDQ method is given in Section 2 of this paper. The formulation of the problem and the basic equations are reported in Section 3. The fundamental system of equations for the parabolic arch is derived according to Hamilton's principle. Section 4 deals with damage modeling. In Section 5, where the most original part of the present study is presented, the equations for the multi-stepped and multi-damaged parabolic arch are reported both in analytical and discrete form. The terms involved in the parabolic arch equations are pointed out and their effect on the structural response are described in Section 6. Section 7 shows final remarks and conclusions.

2 Generalized differential quadrature (GDQ) method

2.1 GDQ review

The GDQ method will be used to discretize the partial space derivatives in the governing equations and boundary conditions. The Differential Quadrature (DQ) method was first presented in the early 1970s. Following the idea of integral quadrature in [25] was suggested to approximate in the partial or total derivative of a smooth function with respect to a variable by a weighted sum of function values at all discrete points in the direction involved by the variable under consideration. The GDQ approach was developed by Shu [33] to improve the DQ technique for the computation of weighting coefficients. It is noted that the weighting coefficients are not related to any special problem and only depend on the grid points and the derivative order. In this methodology various grid distributions can be chosen.

Thus, the $n-th$ order derivative of a function $f(\vartheta)$ with respect to ϑ at a grid point ϑ_i can be approximated with the GDQ approach as follows:

$$\left.\frac{d^n f(\vartheta)}{d\vartheta^n}\right|_{\vartheta=\vartheta_i} \simeq \sum_{j=1}^{\mathcal{N}} \alpha_{ij}^{(n)} f(\vartheta_j), \qquad \text{for} \quad i = 1, 2, \ldots, \mathcal{N} \quad (1)$$

where $\alpha_{ij}^{(n)}$ are the weighting coefficients of the $n-th$ order derivative at the $i-th$ sampling point along the domain. $\mathcal{N}$ is the total number of the sampling points of the grid distribution and $f(\vartheta_j)$ are the function values at the grid points.

The weighting coefficients can be determined by the chosen interpolation rule. In the present study, Lagrange polynomial functions are adopted:

$$p_k(\vartheta) = \frac{\mathcal{L}(\vartheta)}{(\vartheta - \vartheta_k)\mathcal{L}^{(1)}(\vartheta_k)}, \qquad \text{for} \quad k = 1, 2, \ldots, \mathcal{N} \tag{2}$$

where:

$$\begin{aligned} \mathcal{L}(\vartheta) &= \prod_{j=1}^{\mathcal{N}} (\vartheta - \vartheta_j) \\ \mathcal{L}^{(1)}(\vartheta_k) &= \prod_{j=1, j\neq k}^{\mathcal{N}} (\vartheta_k - \vartheta_j) \end{aligned} \tag{3}$$

By applying equation (2) at $\mathcal{N}$ grid points, it is possible to obtain the following algebraic formulations to compute the weighting coefficients α_{ij}:

$$\begin{aligned} \alpha_{ij}^{(1)} &= \frac{\mathcal{L}^{(1)}(\vartheta_i)}{(\vartheta_i - \vartheta_j)\mathcal{L}^{(1)}(\vartheta_j)}, \qquad \text{for} \quad i, j = 1, 2, \ldots, \mathcal{N} \text{ and } i \neq j \\ \alpha_{ii}^{(1)} &= -\sum_{k=1, k\neq i}^{\mathcal{N}} \alpha_{ik}^{(1)}, \qquad \text{for } i = j \end{aligned} \tag{4}$$

The weighting coefficients of the second and higher order derivatives can be computed from a recurrence relationship. A generalized higher order derivative can be written as:

$$\begin{aligned} \alpha_{ij}^{(n)} &= n\left(\alpha_{ii}^{(n-1)}\alpha_{ij}^{(1)} - \frac{\alpha_{ij}^{(n-1)}}{\vartheta_i - \vartheta_j}\right), \\ &\text{for} \quad i \neq j \text{ and} \quad n = 2, 3, \ldots, \mathcal{N} - 1 \\ \alpha_{ii}^{(n)} &= -\sum_{k=1, k\neq i}^{\mathcal{N}} \alpha_{ik}^{(n)}, \qquad \text{for} \quad i = j \end{aligned} \tag{5}$$

2.2 Domain decomposition technique

Any problem of the theory of elasticity having a discontinuity in geometry, material or loading at any point of the domain, can be solved with the GDQ method by using the domain decomposition technique. The present approach was introduced for the first time in [54]. According to this method, the domain of the problem is, at first, divided into a certain number of sub-domains or elements. Then, the GDQ discretization is carried out on each sub-domain. The use of the GDQ method on each sub-domain, together with the use of the domain decomposition technique, is known as the GDQE technique in [30]. More general applications of the present approach include the mapping technique, which is used to map a generic element onto a computational space, in which the solution is carried out. The cited method merges the advantages of the GDQ method and the finite element method. Several complicating problems can be solved by this technique as shown in the papers [55–57].

Thus, the governing differential equations, the inter-element conditions and the actual boundary conditions are defined in discrete form after application of the GDQE technique. Assembling all the discrete fundamental equations, the overall algebraic system can be obtained.

3 Fundamental system of equations

In this paper a Timoshenko parabolic arch is considered, since the shear deformable arch theory follows the theory of the straight Timoshenko beam. The arch center line in a curvilinear coordinate system and the coupling between axial and transverse motions are the main differences between the two theories.

Consider a parabolic arch referred to a global reference system OXY, as shown in Fig. 1a. Let us suppose that the system freely vibrates in the axis plane. The prismatic isotropic arch is characterized by the transverse section area $A = A(\vartheta)$, moment of inertia $I = I(\vartheta)$ about the principal axis of inertia of the arch cross-section, which is parallel to the Z-axis orthogonal to the $X-Y$ plane, radius of curvature $R = R(\vartheta)$ and total angular width $\vartheta_{tot} = |\vartheta^{(A)}| + |\vartheta^{(B)}|$. The angle that the normal at a point P of the curve representing the arch-axis makes with the auxiliary axis of the parabola is denoted by ϑ. A local reference system Pxy is defined with respect to the tangent and the normal to the parabolic mid-line at the generic angle ϑ (see Fig. 1a and Fig. 1b). During vibration, segments representing the cross-sections rotate about the mid-line points. The kinematics of the arch is thoroughly defined by assigning the tangential displacement $u(\vartheta, t)$, the normal displacement $v(\vartheta, t)$ and the rotation angle about the binormal axis $\varphi(\vartheta, t)$.

Fig. 2 shows the parabolic arch with the locus of curvature centres (upon the which three points are highlighted) and the osculating circles for the corresponding points. Table 1 indicates the correspondence among circles, centres and radii under discussion.

Let us consider now a multi-stepped parabolic arch, which freely vibrates in its plane, with small oscillations around an unstressed initial configuration of equilibrium. The system consists of a sequence of n_e consecutive seg-

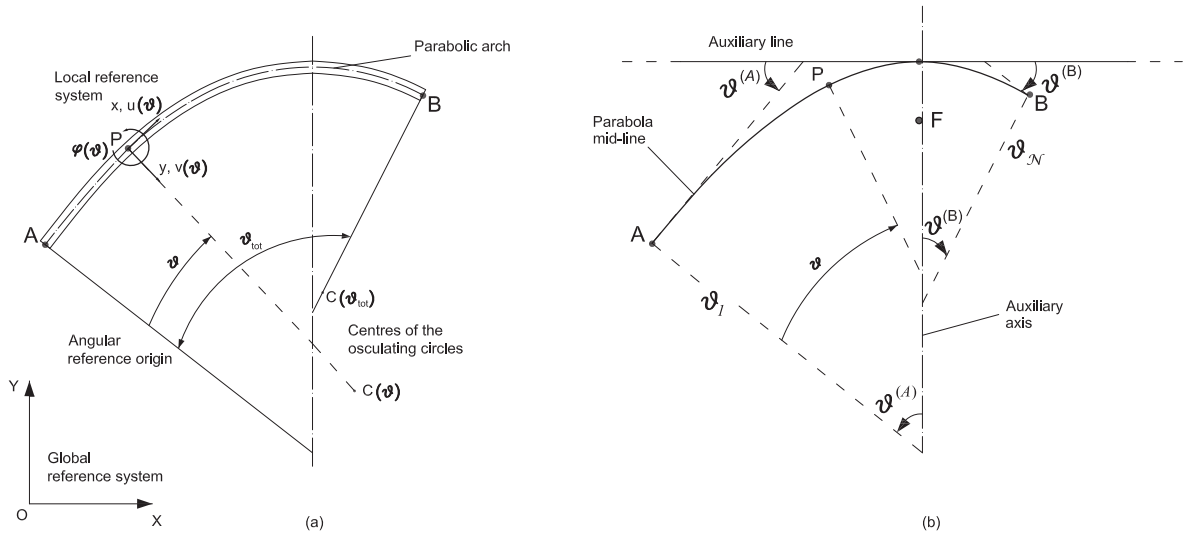

Figure 1: Parabolic arch referred to a global reference system (a). Angle discretization details (b).

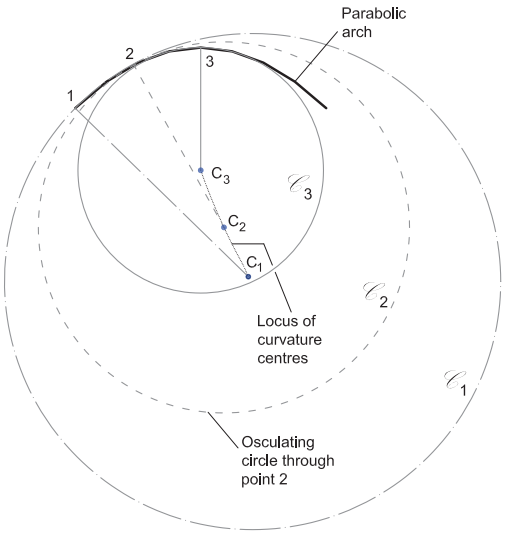

Figure 2: Parabolic arch, osculating circles $\mathcal{C}_1$, $\mathcal{C}_2$, $\mathcal{C}_3$ and corresponding curvature centres C_1, C_2, C_3.

ments. Each arch portion is defined within the angle $\vartheta_1^{(e)} \le \vartheta \le \vartheta_{\mathcal{N}^{(e)}}^{(e)}$ and discretized into $\mathcal{N}^{(e)} = \mathcal{N}$ grid points as shown in Fig. 3, even if, in general, different numbers of grid point $\mathcal{N}^{(e)}$ for each sub-domain can be used; each element can be characterized by a different thickness.

The kinematics of the $e-th$ portion, with $e = 1, \ldots, n_e$, is completely defined by means of the tangential displacement $u^{(e)}(\vartheta, t)$, the normal displacement $v^{(e)}(\vartheta, t)$ and the rotation angle about the binormal axis $\varphi^{(e)}(\vartheta, t)$ at a generic angle $\vartheta_1^{(e)} \le \vartheta \le \vartheta_{\mathcal{N}}^{(e)}$ and time t.

Table 1: Osculating circles, centres and radii for the parabolic arch of Fig. 2.

Arch point	Osculating circle	Osculating circle centre	Osculating circle radius
1	$\mathcal{C}_1$	C_1	$\overline{C_1 1}$
2	$\mathcal{C}_2$	C_2	$\overline{C_2 2}$
3	$\mathcal{C}_3$	C_3	$\overline{C_3 3}$

The strain-displacement relations of the arch are determined using the definitions for the strain-displacements in a curvilinear (polar) coordinate system and can be written as:

$$\begin{aligned}
\varepsilon^{(e)}(\vartheta, t) &= \frac{1}{R^{(e)}(\vartheta)}\left(\frac{\partial u^{(e)}(\vartheta, t)}{\partial \vartheta} - v^{(e)}(\vartheta, t)\right) \\
\gamma^{(e)}(\vartheta, t) &= \frac{1}{R^{(e)}(\vartheta)}\left(\frac{\partial v^{(e)}(\vartheta, t)}{\partial \vartheta} + u^{(e)}(\vartheta, t)\right) + \varphi^{(e)}(\vartheta, t) \\
\kappa^{(e)}(\vartheta, t) &= \frac{1}{R^{(e)}(\vartheta)}\frac{\partial \varphi^{(e)}(\vartheta, t)}{\partial \vartheta}
\end{aligned} \tag{6}$$

where $R^{(e)} = R^{(e)}(\vartheta)$ is the radius of the $e - th$ arch portion. In eq. (6) ε and γ denote the normal and shear strain components, respectively, whereas κ denotes the curvature. It is noticed that the strain-displacement relations (6) are valid for the small displacements hypothesis.

Taking into account the axial-shear deformation effects and the rotatory inertia, the equations of motion are developed using Hamilton principle, which states that

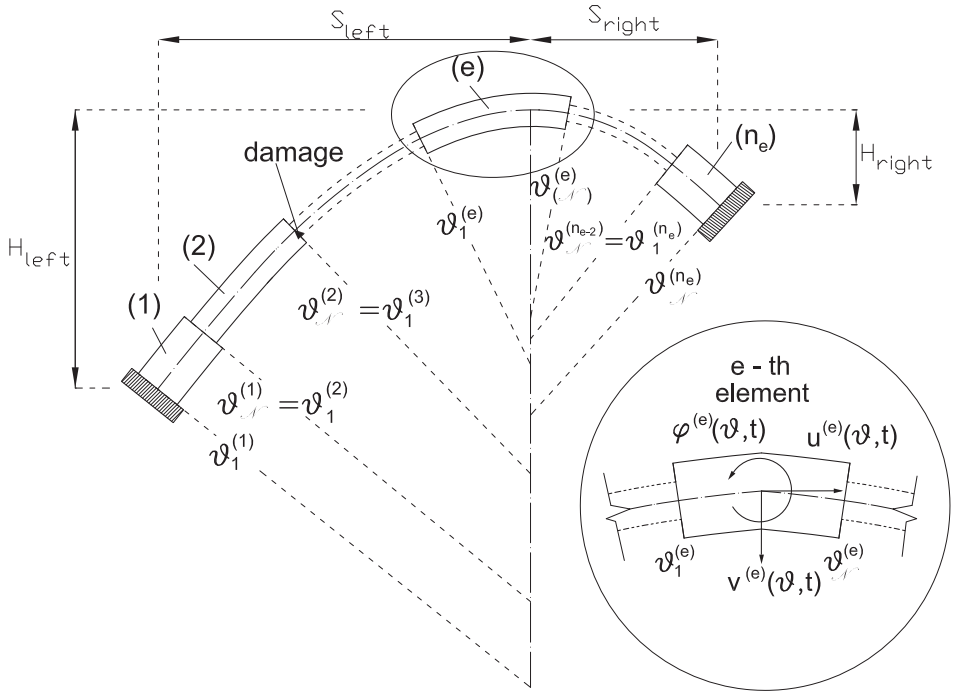

Figure 3: Schematic representation of the multi-stepped parabolic arch.

among the set of all admissible configurations of the system, the actual motion makes the quantity stationary, once the configuration of the system at the limits $t = t_1$ and $t = t_2$ is provided:

$$\delta\Pi = \int_{t_1}^{t_2} \sum_{e=1}^{n_e} \delta\Pi^{(e)} dt = 0 \tag{7}$$

where:

$$\delta\Pi^{(e)} = \int_{t_1}^{t_2} \left(\delta U^{(e)} - \delta T^{(e)} - \delta W_e^{(e)} \right) dt = 0 \tag{8}$$

In (8) $\delta U^{(e)}$, $\delta T^{(e)}$ and $\delta W_e^{(e)}$ are the variations of the strain energy, kinetic energy and work of the external forces for the $e-th$ element, respectively. The strain energy is given by:

$$U^{(e)} = \frac{1}{2} \int_{\vartheta_1^{(e)}}^{\vartheta_N^{(e)}} \left\{ \boldsymbol{\varepsilon}^{(e)} \right\}^T \begin{bmatrix} EA^{(e)} & 0 & 0 \\ 0 & G\Lambda^{(e)} & 0 \\ 0 & 0 & EI^{(e)} \end{bmatrix} \left\{ \boldsymbol{\varepsilon}^{(e)} \right\} d\vartheta \tag{9}$$

where:

$$\left\{ \boldsymbol{\varepsilon}^{(e)} \right\} = \begin{bmatrix} \varepsilon^{(e)}(\vartheta, t) \\ \gamma^{(e)}(\vartheta, t) \\ \kappa^{(e)}(\vartheta, t) \end{bmatrix} \tag{10}$$

In (9) E is the Young's modulus, $G = \frac{E}{2(1+\nu)}$ and $\Lambda = \frac{A}{\chi}$, where χ denotes the shear factor. Analogously, the kinetic energy takes the form:

$$T^{(e)} = \frac{1}{2} \int_{\vartheta_1^{(e)}}^{\vartheta_N^{(e)}} \left\{ \frac{\partial \mathbf{u}^{(e)}}{\partial t} \right\}^T \begin{bmatrix} \rho A^{(e)} & 0 & 0 \\ 0 & \rho A^{(e)} & 0 \\ 0 & 0 & \rho I^{(e)} \end{bmatrix} \frac{\partial \mathbf{u}^{(e)}}{\partial t} d\vartheta \tag{11}$$

where ρ is the mass per volume unit, $A^{(e)}$ and $I^{(e)}$ are the area and the moment of inertia of the cross-section of the $e-th$ arch segment and $\mathbf{u} = \begin{bmatrix} u^{(e)} & v^{(e)} & \varphi^{(e)} \end{bmatrix}^T$ the generalized displacements vector. Finally, the work of the external forces is given by:

$$W_e^{(e)} = \int_{\vartheta_1^{(e)}}^{\vartheta_N^{(e)}} \left\{ \mathbf{u}^{(e)} \right\}^T \mathbf{f}^{(e)} d\vartheta \tag{12}$$

where $\mathbf{f}^{(e)} = \left[f^{(e)} \quad q^{(e)} \quad m^{(e)}\right]^T$ is the vector of the distributed axial and normal forces and distributed moment along the length of the curved beam. The three differential equations of motion are obtained by substituting eqs. (9), (11) and (12) into (8):

$$\begin{aligned}
&\left[\frac{EA^{(e)}}{\left[R^{(e)}\right]^2}\frac{\partial^2}{\partial\vartheta^2} + \left(\frac{E}{\left[R^{(e)}\right]^2}\frac{\partial A^{(e)}}{\partial\vartheta} - \frac{EA^{(e)}}{\left[R^{(e)}\right]^3}\frac{\partial R^{(e)}}{\partial\vartheta}\right)\frac{\partial}{\partial\vartheta} - \frac{G\Lambda^{(e)}}{\left[R^{(e)}\right]^2}\right] u^{(e)}(\vartheta,t) + \\
&- \left[\left(\frac{EA^{(e)}}{\left[R^{(e)}\right]^2} + \frac{G\Lambda^{(e)}}{\left[R^{(e)}\right]^2}\right)\frac{\partial}{\partial\vartheta} + \left(\frac{E}{\left[R^{(e)}\right]^2}\frac{\partial A^{(e)}}{\partial\vartheta} - \frac{EA^{(e)}}{\left[R^{(e)}\right]^3}\frac{\partial R^{(e)}}{\partial\vartheta}\right)\right] v^{(e)}(\vartheta,t) - \frac{G\Lambda^{(e)}}{\left[R^{(e)}\right]}\varphi^{(e)}(\vartheta,t) + f^{(e)}(\vartheta,t) = \rho A^{(e)}\frac{\partial^2 u^{(e)}(\vartheta,t)}{\partial t^2}
\end{aligned}$$

$$\begin{aligned}
&\left[\left(\frac{EA^{(e)}}{\left[R^{(e)}\right]^2} + \frac{G\Lambda^{(e)}}{\left[R^{(e)}\right]^2}\right)\frac{\partial}{\partial\vartheta} + \left(\frac{G}{\left[R^{(e)}\right]^2}\frac{\partial\Lambda^{(e)}}{\partial\vartheta} - \frac{G\Lambda^{(e)}}{\left[R^{(e)}\right]^3}\frac{\partial}{\partial\vartheta}\right)\right] u^{(e)}(\vartheta,t) + \\
&+ \left[\frac{G\Lambda^{(e)}}{\left[R^{(e)}\right]^2}\frac{\partial^2}{\partial\vartheta^2} + \left(\frac{G}{\left[R^{(e)}\right]^2}\frac{\partial\Lambda^{(e)}}{\partial\vartheta} - \frac{G\Lambda^{(e)}}{\left[R^{(e)}\right]^3}\frac{\partial R^{(e)}}{\partial\vartheta}\right)\frac{\partial}{\partial\vartheta} - \frac{EA^{(e)}}{\left[R^{(e)}\right]^2}\right] v^{(e)}(\vartheta,t) + \\
&+ \left[\frac{G\Lambda^{(e)}}{\left[R^{(e)}\right]}\frac{\partial}{\partial\vartheta} + \frac{G}{\left[R^{(e)}\right]}\frac{\partial\Lambda^{(e)}}{\partial\vartheta}\right]\varphi^{(e)}(\vartheta,t) + q^{(e)}(\vartheta,t) = \rho A^{(e)}\frac{\partial^2 v^{(e)}(\vartheta,t)}{\partial t^2}
\end{aligned}$$

$$\begin{aligned}
&\left[-\frac{G\Lambda^{(e)}}{\left[R^{(e)}\right]}\right] u^{(e)}(\vartheta,t) - \left[\frac{G\Lambda^{(e)}}{\left[R^{(e)}\right]}\frac{\partial}{\partial\vartheta}\right] v^{(e)}(\vartheta,t) + \\
&+ \left[\frac{EI^{(e)}}{\left[R^{(e)}\right]^2}\frac{\partial^2}{\partial\vartheta^2} + \left(\frac{E}{\left[R^{(e)}\right]^2}\frac{\partial I^{(e)}}{\partial\vartheta} - \frac{EI^{(e)}}{\left[R^{(e)}\right]^3}\frac{\partial R^{(e)}}{\partial\vartheta}\right)\frac{\partial}{\partial\vartheta} - G\Lambda^{(e)}\right]\varphi^{(e)}(\vartheta,t) + m^{(e)}(\vartheta,t) = \rho I^{(e)}\frac{\partial^2\varphi^{(e)}(\vartheta,t)}{\partial t^2}
\end{aligned} \tag{13}$$

It should be noted that in the case of circular arches the following terms of (13), which are the derivative with respect to ϑ, do not appear:

$$\frac{\partial R^{(e)}}{\partial\vartheta} = 0, \qquad \frac{\partial A^{(e)}}{\partial\vartheta} = 0, \qquad \frac{\partial\Lambda^{(e)}}{\partial\vartheta} = 0, \qquad \frac{\partial I^{(e)}}{\partial\vartheta} = 0 \tag{14}$$

In other words, the formulation (13) allows one to take into account the variability of the radius and cross-section along the arch axis.

In addition, continuity and equilibrium conditions between the $e-th$ and the $(e+1)-th$ arch portions at a generic angle ϑ must be introduced:

$$\begin{aligned}
u^{(e+1)}(\vartheta,t) &= u^{(e)}(\vartheta,t), \\
v^{(e+1)}(\vartheta,t) &= v^{(e)}(\vartheta,t), \\
\varphi^{(e+1)}(\vartheta,t) &= \varphi^{(e)}(\vartheta,t), \\
N^{(e+1)}(\vartheta,t) &= N^{(e)}(\vartheta,t), \\
T^{(e+1)}(\vartheta,t) &= T^{(e)}(\vartheta,t), \\
M^{(e+1)}(\vartheta,t) &= M^{(e)}(\vartheta,t)
\end{aligned} \tag{15}$$

External boundary conditions are imposed at $\vartheta_1^{(1)}$ and $\vartheta_{\mathcal{N}}^{(n_e)}$.

If the arch extreme is clamped, then the boundary condition, for $t > 0$, takes the form:

$$\begin{aligned}
u^{(e)}(\vartheta,t) &= 0, \\
v^{(e)}(\vartheta,t) &= 0, \\
\varphi^{(e)}(\vartheta,t) &= 0
\end{aligned} \tag{16}$$

If the arch extreme is hinged, the boundary condition, for $t > 0$, can be expressed in the form:

$$\begin{aligned} u^{(e)}(\vartheta, t) &= 0, \\ v^{(e)}(\vartheta, t) &= 0, \\ M^{(e)}(\vartheta, t) &= 0 \end{aligned} \tag{17}$$

Finally, if the arch extreme is free, the boundary condition, for $t > 0$, assumes the aspect:

$$\begin{aligned} N^{(e)}(\vartheta, t) &= 0, \\ T^{(e)}(\vartheta, t) &= 0, \\ M^{(e)}(\vartheta, t) &= 0 \end{aligned} \tag{18}$$

4 Damage modeling

As it is well known from [58], damage in a beam introduces a local flexibility that affects its mechanical response. In order to study the behaviour of a damaged structure, a suitable model for the notched section is required. Hereinafter, the mechanical behaviour of the damaged section is reproduced as an ad hoc internal constraint characterized by three elastic spring constants simulating axial, transversal and flexural deformations (see Fig. 4).

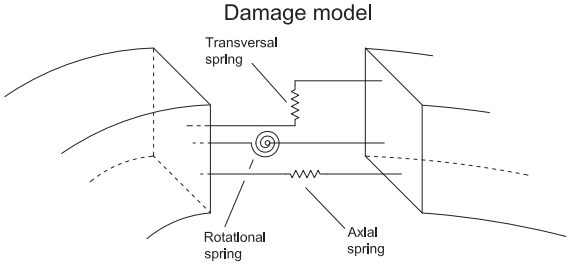

Figure 4: Schematic representation of the damage modelling.

The damaged cross-section can be modelled by three massless springs [59–61] having axial K_a, normal K_t and rotational K_r elastic stiffnesses that range from zero to infinite. Each spring stiffness can be related to the damage geometry, as discussed in [4] and [7]. Infinite spring stiffness means that there is no damage and material continuity is re-established. On the other hand, a spring stiffness of finite value signifies the presence of damage in the cross-section. The stiffness values considered turn in damage severity according to the following laws:

$$\begin{aligned} K_a &= \frac{EA^D}{EA - EA^D}\frac{EA}{s_{dam}}, \\ K_t &= \frac{G\Lambda^D}{G\Lambda - G\Lambda^D}\frac{G\Lambda}{s_{dam}}, \\ K_r &= \frac{EI^D}{EI - EI^D}\frac{EI}{s_{dam}} \end{aligned} \tag{19}$$

where EA^D, $G\Lambda^D$ and EI^D are the axial, transversal and bending stiffnesses of the notched cross-section and s_{dam} is the longitudinal extension of the notch. As it can be read in [4], when the damage does not extend for a long path the notch length can be calculated as $s_{dam} = R^{obs}\Delta\vartheta$, where R^{obs} is the curvature radius of the osculating circle for the damage mid-point, and $\Delta\vartheta$ is the opening angle of the notch.

When a notch is located at a generic cross-section, between the $e - th$ and the $(e + 1) - th$ arch portions, the continuity conditions (15) are replaced by:

$$\begin{aligned} K_a\left[u^{(e+1)}(\vartheta, t) - u^{(e)}(\vartheta, t)\right] &= N^{(e)}(\vartheta, t), \\ K_t\left[v^{(e+1)}(\vartheta, t) - v^{(e)}(\vartheta, t)\right] &= T^{(e)}(\vartheta, t), \\ K_r\left[\varphi^{(e+1)}(\vartheta, t) - \varphi^{(e)}(\vartheta, t)\right] &= M^{(e)}(\vartheta, t), \\ N^{(e+1)}(\vartheta, t) &= N^{(e)}(\vartheta, t), \\ T^{(e+1)}(\vartheta, t) &= T^{(e)}(\vartheta, t), \\ M^{(e+1)}(\vartheta, t) &= M^{(e)}(\vartheta, t) \end{aligned} \tag{20}$$

for $t > 0$. It is worth noting that in this study the axial and transversal stiffness of the modelled springs are also taken into account.

From a computational point of view, when the notch appears at a generic angle $\vartheta_1^{(e)} < \vartheta < \vartheta_{\mathcal{N}}^{(e)}$ of the $e - th$ arch portion, then the arch portion is split into two parts and the corresponding equations of motions (13) must be written separately for the two parts, $(\vartheta_1^{(e)}, \vartheta)$ and $(\vartheta, \vartheta_{\mathcal{N}}^{(e)})$, located on the left and on the right side of the notch, respectively.

A multi-stepped arch with an arbitrary number of notches can be considered by arranging, in a proper set, the boundary conditions (16), (17) or (18) and the continuity conditions (15) or (20) between two consecutive segments.

5 Analytical statement of the problem and numerical implementation

5.1 Analytical statement of the problem

Let us firstly consider the case of a multi-stepped arch in its undamaged configuration. The governing equations of free vibrations are given by the coupled system of partial differential equations (13), with boundary conditions (16)-(18) in the case of Clamped-Clamped, Hinged-Hinged or Clamped-Free ends, respectively, and with the continuity conditions (15). We seek solutions that are harmonic in time and characterized by frequency ω; then, in each arch portion, the displacements and the rotation can be written as:

$$\begin{aligned} u^{(e)}(\vartheta, t) &= U^{(e)}(\vartheta)\cos(\omega t), \\ v^{(e)}(\vartheta, t) &= V^{(e)}(\vartheta)\cos(\omega t), \\ \varphi^{(e)}(\vartheta, t) &= \Phi^{(e)}(\vartheta)\cos(\omega t) \end{aligned} \tag{21}$$

for $\vartheta \in [\vartheta_1^{(e)}, \vartheta_{\mathcal{N}}^{(e)}]$, $t \geq 0$ and $e = 1, \ldots, n_e$, where the vibration spatial amplitude values $U^{(e)}$, $V^{(e)}$, $\Phi^{(e)}$ satisfy the differential system reported in Appendix B. Appendix B discusses in detail other mathematical steps of the formulation.

5.2 Numerical implementation

The aforementioned assumptions allow us to write the equations of motion in discrete form, transforming every derivative space into a weighted sum of nodal values of dependent variables by applying the GDQ procedure. Each equation is valid in a single sampling point belonging to one of the arch segments. For the generic arch portion "e" and its interior sampling points, $i = 2, 3, \cdots \mathcal{N}^{(e)} - 1$, the governing eqs. (13) can be discretized as follows:

$$\begin{aligned}
&\left[\frac{EA_i^{(e)}}{\left[R_i^{(e)}\right]^2}\sum_{j=1}^{\mathcal{N}^{(e)}}\alpha_{ij}^{(2)(e)}U_j^{(e)} + \left(\frac{E}{\left[R_i^{(e)}\right]^2}\sum_{j=1}^{\mathcal{N}^{(e)}}\alpha_{ij}^{(1)(e)}A_j^{(e)} - \frac{EA_i^{(e)}}{\left[R_i^{(e)}\right]^3}\sum_{j=1}^{\mathcal{N}^{(e)}}\alpha_{ij}^{(1)(e)}R_j^{(e)}\right)\sum_{j=1}^{\mathcal{N}^{(e)}}\alpha_{ij}^{(1)(e)}U_j^{(e)} - \frac{G\Lambda_i^{(e)}}{\left[R_i^{(e)}\right]^2}U_i^{(e)}\right] + \\
&- \left[\left(\frac{EA_i^{(e)}}{\left[R_i^{(e)}\right]^2} + \frac{G\Lambda_i^{(e)}}{\left[R_i^{(e)}\right]^2}\right)\sum_{j=1}^{\mathcal{N}^{(e)}}\alpha_{ij}^{(1)(e)}V_j^e + \right. \\
&\left. + \left(\frac{E}{\left[R_i^{(e)}\right]^2}\sum_{j=1}^{\mathcal{N}^{(e)}}\alpha_{ij}^{(1)(e)}A_j^{(e)} - \frac{EA_i^{(e)}}{\left[R_i^{(e)}\right]^3}\sum_{j=1}^{\mathcal{N}^{(e)}}\alpha_{ij}^{(1)(e)}R_j^{(e)}\right)V_i^{(e)}\right] - \frac{G\Lambda_i^{(e)}}{R_i^{(e)}}\Phi_i^{(e)} = -\omega^2\rho A_i^{(e)}U_i^{(e)} \\
&\left[\left(\frac{EA_i^{(e)}}{\left[R_i^{(e)}\right]^2} + \frac{G\Lambda_i^{(e)}}{\left[R_i^{(e)}\right]^2}\right)\sum_{j=1}^{\mathcal{N}^{(e)}}\alpha_{ij}^{(1)(e)}U_j^{(e)} + \left(\frac{G}{\left[R_i^{(e)}\right]^2}\sum_{j=1}^{\mathcal{N}^{(e)}}\alpha_{ij}^{(1)(e)}\Lambda_j^{(e)} - \frac{G\Lambda_i^{(e)}}{\left[R_i^{(e)}\right]^3}\sum_{j=1}^{\mathcal{N}^{(e)}}\alpha_{ij}^{(1)(e)}\right)U_i^{(e)}\right] + \\
&+ \left[\frac{G\Lambda_i^{(e)}}{\left[R_i^{(e)}\right]^2}\sum_{j=1}^{\mathcal{N}^{(e)}}\alpha_{ij}^{(2)(e)}V_j^{(e)} + \left(\frac{G}{\left[R_i^{(e)}\right]^2}\sum_{j=1}^{\mathcal{N}^{(e)}}\alpha_{ij}^{(1)(e)}\Lambda_j^{(e)} - \frac{G\Lambda_i^{(e)}}{\left[R_i^{(e)}\right]^3}\sum_{j=1}^{\mathcal{N}^{(e)}}\alpha_{ij}^{(1)(e)}R_j^{(e)}\right)\sum_{j=1}^{\mathcal{N}^{(e)}}\alpha_{ij}^{(1)(e)}V_j^{(e)} - \frac{EA_i^{(e)}}{\left[R_i^{(e)}\right]^2}V_i^{(e)}\right] + \\
&+ \left[\frac{G\Lambda_i^{(e)}}{R_i^{(e)}}\sum_{j=1}^{\mathcal{N}^{(e)}}\alpha_{ij}^{(1)(e)}\Phi_j^{(e)} + \frac{G}{R_i^{(e)}}\sum_{j=1}^{\mathcal{N}^{(e)}}\alpha_{ij}^{(1)(e)}\Lambda_j^{(e)}\Phi_i^{(e)}\right] = -\omega^2\rho A_i^{(e)}V_i^{(e)} \\
&\left[-\frac{G\Lambda_i^{(e)}}{R_i^{(e)}}\right]U_i^{(e)} - \left[\frac{G\Lambda_i^{(e)}}{R_i^{(e)}}\sum_{j=1}^{\mathcal{N}^{(e)}}\alpha_{ij}^{(1)(e)}\right]V_i^{(e)} + \\
&+ \left[\frac{EI_i^{(e)}}{\left[R_i^{(e)}\right]^2}\sum_{j=1}^{\mathcal{N}^{(e)}}\alpha_{ij}^{(2)(e)}\Phi_j^{(e)} + \left(\frac{E}{\left[R_i^{(e)}\right]^2}\sum_{j=1}^{\mathcal{N}^{(e)}}\alpha_{ij}^{(1)(e)}I_j^{(e)} - \frac{EI_i^{(e)}}{\left[R_i^{(e)}\right]^3}\sum_{j=1}^{\mathcal{N}^{(e)}}\alpha_{ij}^{(1)(e)}R_j^{(e)}\right)\sum_{j=1}^{\mathcal{N}^{(e)}}\alpha_{ij}^{(1)(e)}\Phi_j^{(e)} - G\Lambda_i^{(e)}\Phi_i^{(e)}\right] = -\omega^2\rho I_i^{(e)}\Phi_i^{(e)}
\end{aligned} \tag{22}$$

In (22), the variable α has superscripts (that denote the order of the weighting coefficient and the element processed) and subscripts (that indicate the processed point). Furthermore, it appears from (22) that the discretized equations are different from the ones reported by [21] for the circular arch.

Applying the GDQ methodology, the discretized forms of the boundary conditions are given below:

- Clamped edge boundary condition:

$$\begin{aligned} U_i^{(e)} &= 0, \\ V_i^{(e)} &= 0, \\ \Phi_i^{(e)} &= 0, \end{aligned} \tag{23}$$

- Hinged edge boundary condition:

$$\begin{aligned} U_i^{(e)} &= 0, \\ V_i^{(e)} &= 0, \\ \sum_{j=1}^{\mathcal{N}^{(e)}} \alpha_{ij}^{(1)(e)} \Phi_j^{(e)} &= 0, \end{aligned} \tag{24}$$

- Free edge boundary condition:

$$\begin{aligned} &\sum_{j=1}^{\mathcal{N}^{(e)}} \alpha_{ij}^{(1)(e)} U_j^{(e)} - V_i^{(e)} = 0, \\ &U_i^{(e)} + \sum_{j=1}^{\mathcal{N}^{(e)}} + \alpha_{ij}^{(1)(e)} V_j^{(e)} + R_i^{(e)} \Phi_i^{(e)} = 0, \\ &\sum_{j=1}^{\mathcal{N}^{(e)}} \alpha_{ij}^{(1)(e)} \Phi_j^{(e)} = 0, \end{aligned} \tag{25}$$

It is worth noting that $j = 1 \cdots \mathcal{N}$ while i and e can assume the following values:

i) $i = 1, e = 1$ when the constraint is applied at the left end of the arch;
ii) $i = \mathcal{N}, e = n_e$ when the constraint is applied at the right end of the arch.

For each discontinuity the jump conditions (20) are:

$$\begin{aligned} U_1^{(e+1)} &= U_{\mathcal{N}^{(e)}}^{(e)}, \\ V_1^{(e+1)} &= V_{\mathcal{N}^{(e)}}^{(e)}, \\ \Phi_1^{(e+1)} &= \Phi_{\mathcal{N}^{(e)}}^{(e)}, \end{aligned}$$

$$\begin{aligned} &\frac{EA_1^{(e+1)}}{R_1} \left(\sum_{j=1}^{\mathcal{N}^{(e+1)}} \alpha_{1j}^{(1)(e+1)} U_j^{(e+1)} - V_1^{(e+1)} \right) = \\ &= \frac{EA_{\mathcal{N}^{(e)}}^{(e)}}{R_{\mathcal{N}^{(e)}}} \left(\sum_{j=1}^{\mathcal{N}^{(e)}} \alpha_{\mathcal{N}^{(e)}j}^{(1)(e)} U_j^{(e)} - V_{\mathcal{N}^{(e)}}^{(e)} \right), \\ &\frac{G\Lambda_1^{(e+1)}}{R_1} \left(U_1^{(e+1)} + \sum_{j=1}^{\mathcal{N}^{(e+1)}} + \alpha_{1j}^{(1)(e+1)} V_j^{(e+1)} + R_1 \Phi_1^{(e+1)} \right) = \\ &= \frac{G\Lambda_{\mathcal{N}^{(e)}}^{(e)}}{R_{\mathcal{N}^{(e)}}} \left(U_{\mathcal{N}^{(e)}}^{(e)} + \sum_{j=1}^{\mathcal{N}^{(e)}} \alpha_{\mathcal{N}^{(e)}j}^{(1)(e)} V_j^{(e)} + R_{\mathcal{N}^{(e)}} \Phi_{\mathcal{N}^{(e)}}^{(e)} \right), \\ &\frac{EI_1^{(e+1)}}{R_1} \sum_{j=1}^{\mathcal{N}^{(e+1)}} \alpha_{1j}^{(1)(e+1)} \Phi_j^{(e+1)} = \frac{EI_{\mathcal{N}^{(e)}}^{(e)}}{R_{\mathcal{N}^{(e)}}} \sum_{j=1}^{\mathcal{N}^{(e)}} \alpha_{\mathcal{N}^{(e)}j}^{(1)(e)} \Phi_j^{(e)} \end{aligned} \tag{26}$$

It is noted that, in the case of circular arches, the last three equations yield $R_1 = R_{\mathcal{N}^{(e)}} = R$. For parabolic arches the radius is not constant, and varies along the arch. The subscript of variable R, which denotes the radius of curvature, represents one of the innovative aspect of the present paper.

In presence of a damage, the first three equations (26) must be re-written as:

$$\begin{aligned} &K_a \left[U_1^{(e+1)} - U_{\mathcal{N}^{(e)}}^{(e)} \right] = \frac{EA_{\mathcal{N}^{(e)}}^{(e)}}{R_{\mathcal{N}^{(e)}}} \left(\sum_{j=1}^{\mathcal{N}^{(e)}} \alpha_{\mathcal{N}^{(e)}j}^{(1)(e)} U_j^{(e)} - V_{\mathcal{N}^{(e)}}^{(e)} \right), \\ &K_t \left[V_1^{(e+1)} - V_{\mathcal{N}^{(e)}}^{(e)} \right] = \\ &= \frac{G\Lambda_{\mathcal{N}^{(e)}}^{(e)}}{R_{\mathcal{N}^{(e)}}} \left(U_{\mathcal{N}^{(e)}}^{(e)} + \sum_{j=1}^{\mathcal{N}^{(e)}} \alpha_{\mathcal{N}^{(e)}j}^{(1)(e)} V_j^{(e)} + R_{\mathcal{N}^{(e)}} \Phi_{\mathcal{N}^{(e)}}^{(e)} \right), \\ &K_r \left[\Phi_1^{(e+1)} - \Phi_{\mathcal{N}^{(e)}}^{(e)} \right] = \frac{EI_{\mathcal{N}^{(e)}}^{(e)}}{R_{\mathcal{N}^{(e)}}} \sum_{j=1}^{\mathcal{N}^{(e)}} \alpha_{\mathcal{N}^{(e)}j}^{(1)(e)} \Phi_j^{(e)} \end{aligned} \tag{27}$$

Applying the GDQE procedure in a similar manner to as it was presented in [62, 63] the whole system of differential equations can be discretized, and the global assembling leads to the following set of linear algebraic equations:

$$\begin{bmatrix} \mathbf{K}_{bb} & \mathbf{K}_{bd} \\ \mathbf{K}_{db} & \mathbf{K}_{dd} \end{bmatrix} \begin{bmatrix} \boldsymbol{\delta}_b \\ \boldsymbol{\delta}_d \end{bmatrix} = \omega^2 \begin{bmatrix} \mathbf{0} & \mathbf{0} \\ \mathbf{0} & \mathbf{M}_{dd} \end{bmatrix} \begin{bmatrix} \boldsymbol{\delta}_b \\ \boldsymbol{\delta}_d \end{bmatrix} \tag{28}$$

In the above matrices and vectors, the subscripts b and d refer to degrees of freedom of the boundary and the domain, respectively. In order to make the computation

more efficient, kinematic condensation of non-domain degrees of freedom is performed:

$$\left(\mathbf{K}_{dd} - \mathbf{K}_{db}\left(\mathbf{K}_{bb}\right)^{-1}\mathbf{K}_{bd}\right)\boldsymbol{\delta}_d = \omega^2\mathbf{M}_{dd}\boldsymbol{\delta}_d \qquad (29)$$

The natural frequencies of the structure can be determined by making the following determinant equal to zero:

$$\left|\left(\mathbf{K}_{dd} - \mathbf{K}_{db}\left(\mathbf{K}_{bb}\right)^{-1}\mathbf{K}_{bd}\right) - \omega^2\mathbf{M}_{dd}\right| = 0 \qquad (30)$$

6 Numerical applications

In the present paragraph some results and considerations about the free vibration problem of damaged and undamaged multi-stepped as well as multi-damaged parabolic arches with different boundary conditions are presented. The natural frequencies for the circular arch reported in [21] are considered as a benchmark to test the reliability of the proposed formulation. The formulation for the parabolic arch is validated by comparing the code frequencies with those obtained by a commercial software.

The coordinates of grid points are chosen as follows:

$$\vartheta_i^{(e)} = \frac{1 - \cos\left[\frac{\pi(i-1)}{\mathcal{N}-1}\right]}{2}\left(\vartheta_1^{(e)} - \vartheta_{\mathcal{N}}^{(e)}\right), \qquad \text{for} \quad i = 1, \cdots, \mathcal{N} \qquad (31)$$

where $(\vartheta_1^{(e)} - \vartheta_{\mathcal{N}}^{(e)})$ and $\mathcal{N}^{(e)} = \mathcal{N}$ are the amplitude of the $e - th$ arch portion (see Fig. 3) and the total number of sampling points used to discretize it, respectively. In the present work, the same number of sampling points $\mathcal{N}^{(e)} = \mathcal{N}$ for each sub-domain "e" is used. This sampling method is known as the *Chebyshev-Gauss-Lobatto sampling point rule* (31). Combining Lagrange interpolating polynomials (2) with the Chebyshev-Gauss-Lobatto sampling point rule provides a simple and highly efficient numerical technique, as shown in details in [64–67].

6.1 Circular arches

Firstly, a circular steel arch is considered. The steel is modelled as an isotropic elastic material. The mechanical and geometrical properties of the considered arches are reported in table 2. The full amplitude of the symmetric arch is $\vartheta_{tot} = 120^\circ$.

Table 3 shows the first 10 eigenfrequencies for the analogous cases examined in [21]. Two examples are considered: Clamped-Clamped and Hinged-Hinged circular arch with constant rectangular cross-section (b =

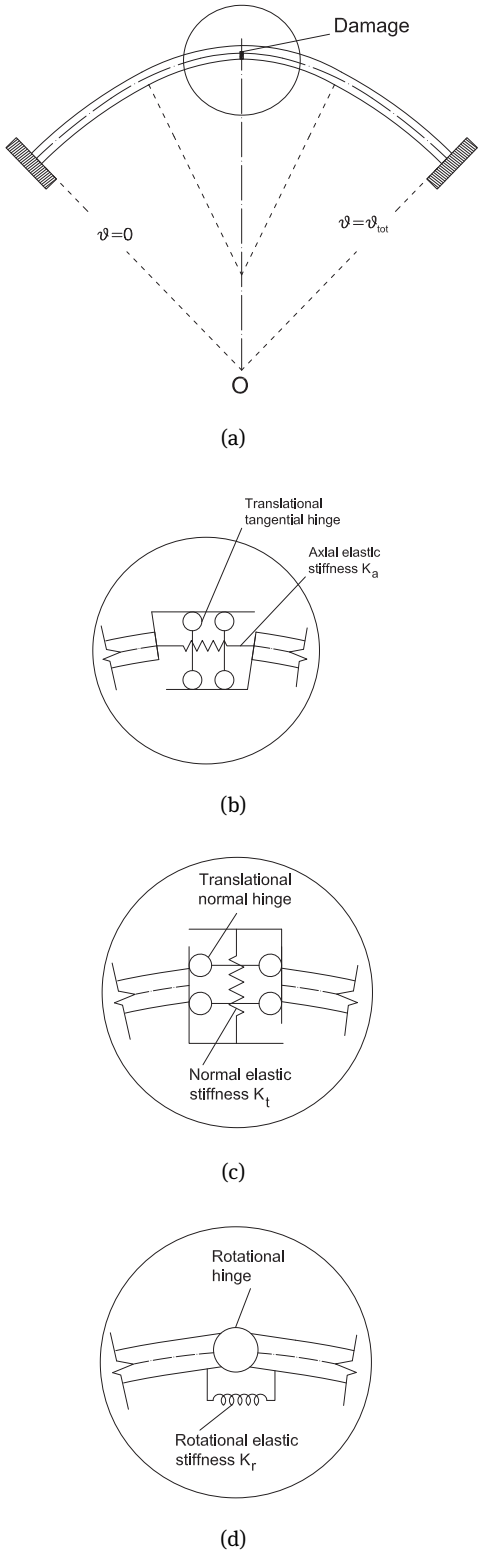

Figure 5: (a) Parabolic arch with a notch in the key section. The notch is modelled as: (b) a translational tangential elastic hinge; (c) a translational normal elastic hinge; (d) a rotational elastic hinge.

Table 2: Mechanical and geometrical parameters used in the free vibrations analysis.

Mechanical and geometrical properties of the arch						
Mechanical properties			Geometrical properties			
					Value	
Property	Symbol	Value	Property	Symbol	Circular arch	Parabolic arch
Mass density	ρ	7850 kg/m^3	Left span	S_{left}	1 m	1 m
Young's modulus	E	$2.1 \cdot 10^{11}$ Pa	Right span	S_{right}	1 m	1 m
Poisson's ratio	ν	0.3	Left rise	H_{left}	1 m	1 m
Shear factor	χ	1.2	Right rise	H_{right}	1 m	1 m

0.045 m, h = 0.020 m). Table 3 also reports natural frequencies for damaged arches. An arch with a three-stepped cross-section is examined: arch segments near the ends are characterized by the thickness $h^{(1)} = h^{(3)} =$ 0.020m and sweep angle $\vartheta_{\mathcal{N}}^{(1)} - \vartheta_1^{(1)} = \vartheta_{\mathcal{N}}^{(3)} - \vartheta_1^{(3)} = 30^\circ$, while the middle arch segment has thickness $h^{(2)} = 0.015$m and sweep angle $\vartheta_{\mathcal{N}}^{(2)} - \vartheta_1^{(2)} = 60^\circ$. In the damaged arch the notch is located at $\vartheta = 60^\circ$ and has a depth of 5mm, corresponding to a rotational elastic stiffness $K_r = 217.31$ kNm. The results presented in table 3 have recently been cited for comparison by [68].

6.2 Undamaged parabolic arches

In this section, parabolic arches are examined. The mechanical properties of the arches are reported in table 2.

Firstly, an undamaged parabolic arch is considered: table 4 shows the first ten frequencies for three different boundary conditions: Clamped-Clamped, Hinged-Hinged and Clamped-Free. The arch is characterized by a rectangular constant cross-section (b = 0.045m and h = 0.020m) and $\vartheta_{tot} = 120^\circ$. The results are compared with those obtained by using ABAQUS (discretizing the arch by 676 quadratic line elements of type B22).

A three-stepped parabolic arch is also investigated, in which the cross-sectional changes occur at $0.25\vartheta_{tot}$ and $0.75\vartheta_{tot}$. It is noticed that $0.25\vartheta_{tot}$ does not correspond to $0.25s_0$, where s_0 is the arch mid-line length, since the axis of the arch is parabolic. The arch segments near the ends are characterized by the same thickness, $h^{(1)} = h^{(3)} = 0.020$ m while the middle one has thickness $h^{(2)} = 0.015$ m. The results shown in table 5 are compared with those obtained by means of ABAQUS using the same mesh as adopted before (676 quadratic line elements of type B22). The good agreement confirms once again the reliability of the code.

This

6.3 Damaged parabolic arches

Finally, damaged parabolic arches are examined. The localized damage is introduced by placing a notch at the cross-sectional level. At first, a single notch in the key section is introduced, and the damage is modelled as elastic springs having only one degree of freedom each. Each spring only reacts to one translational displacement or rotation, as shown in Fig. 5. The stiffnesses of the elastic hinges are K_a and K_t for translational tangential or normal displacements and K_r for rotations. Numerical results are presented in Fig. 6, where each of the curves shown refers, in turn, to the variability of the stiffness of one spring, whereas the other two springs are assumed to have infinite rigidity.

Axial and normal elastic stiffnesses are expressed in [N/m], while rotational elastic stiffness measure units are [Nm]. The twelve curves shown in Fig. 6 range from 0 to 900 Hz. Each curve converges to a particular value (right part of the graphic) that represents the highest possible value for that mode and coincides with the vibrating frequency value for the pristine case (see table 6 for infinitive stiffness values).

It appears that the majority of the frequencies assume the lowest constant values (i.e. vibrating modes are practically independent of the notch severity) in the $[0 - 10^4]$ stiffness range. Here, the vibrating modes can be defined as *stiffness independent* since stiffness increments do not cause any variation in frequency. On the other hand, material continuity is re-established for different stiffness values depending on the different modes (lower stiffness values for the first modes and higher stiffness values for the last modes). Frequencies assume the highest possible value when the spring stiffness is so high that there is practically no discontinuity. The discontinuity disappears for different stiffness values when different modes and kind of spring are considered.

Table 3: Comparison between the analytical solution and the current in-house code values for the first 10 natural frequencies of an undamaged and a damaged three-stepped circular arch.

	Undamaged circular arch				Damaged circular arch			
	Clamped-Clamped		Hinged-Hinged		Clamped-Clamped		Hinged-Hinged	
Mode number	Viola et al. (2007) [Hz]	GDQE present [Hz]	Viola et al. (2007) [Hz]	GDQE present [Hz]	Viola et al. (2007) [Hz]	GDQE present [Hz]	Viola et al. (2007) [Hz]	GDQE present [Hz]
1	49.535	49.535	27.564	27.564	49.535	49.535	27.564	27.564
2	99.224	99.224	74.838	74.838	98.603	98.603	74.397	74.397
3	178.742	178.742	140.321	140.321	178.742	178.742	140.321	140.321
4	261.989	261.989	215.215	215.215	260.529	260.529	214.005	214.005
5	366.855	366.855	313.167	313.167	366.855	366.855	313.167	313.167
6	485.004	485.004	432.367	432.367	482.111	482.111	429.709	429.709
7	646.009	646.009	576.539	576.539	646.009	646.009	576.539	576.539
8	732.315	732.321	698.877	698.879	730.251	730.251	695.638	695.638
9	865.512	865.512	823.817	823.815	862.631	862.631	822.885	822.885
10	969.683	969.694	882.598	882.603	969.683	969.694	882.598	882.598

Table 4: Comparison between the ABAQUS solution and the current in-house code values for the first 10 natural frequencies for undamaged constant cross-section parabolic arches.

Mode	Clamped-Clamped			Hinged-Hinged			Clamped-Free		
number	ABAQUS [Hz]	GDQE [Hz]	Δ [%]	ABAQUS [Hz]	GDQE [Hz]	Δ [%]	ABAQUS [Hz]	GDQE [Hz]	Δ [%]
1	25.303	25.302	0.006	14.980	14.978	0.010	2.380	2.380	0.002
2	58.319	58.314	0.008	41.252	41.248	0.009	6.853	6.853	0.006
3	101.190	101.179	0.011	78.708	78.702	0.008	26.930	26.928	0.006
4	152.590	152.567	0.015	125.310	125.292	0.014	58.301	58.296	0.008
5	216.260	216.260	0.000	183.700	183.680	0.011	101.120	101.114	0.006
6	290.330	290.335	0.002	252.540	252.525	0.006	153.180	153.157	0.015
7	374.640	374.543	0.026	331.710	331.644	0.020	216.660	216.647	0.006
8	468.170	467.829	0.073	420.650	420.470	0.043	290.650	290.637	0.004
9	573.070	572.787	0.049	520.380	520.241	0.027	374.870	374.779	0.024
10	671.910	671.741	0.025	629.620	629.774	0.024	469.030	468.752	0.059

Table 5: Comparison between the ABAQUS solution and the current in-house code values for the first 10 natural frequencies of undamaged three-stepped parabolic arches.

Mode	Clamped-Clamped			Hinged-Hinged			Clamped-Free		
number	ABAQUS [Hz]	GDQE [Hz]	Δ [%]	ABAQUS [Hz]	GDQE [Hz]	Δ [%]	ABAQUS [Hz]	GDQE [Hz]	Δ [%]
1	24.458	24.416	0.172	14.541	14.515	0.010	2.230	2.229	0.049
2	58.319	58.314	0.008	41.252	41.248	0.009	5.677	5.670	0.129
3	101.190	101.179	0.011	78.708	78.702	0.008	25.514	25.456	0.229
4	152.590	152.567	0.015	125.310	125.292	0.014	53.975	53.974	0.002
5	216.260	216.260	0.000	183.700	183.680	0.011	92.332	92.178	0.167
6	290.330	290.335	0.002	252.540	252.525	0.006	144.550	144.334	0.150
7	374.640	374.543	0.026	331.710	331.644	0.020	201.100	201.089	0.005
8	468.170	467.829	0.073	420.650	420.470	0.043	269.920	269.323	0.221
9	573.070	572.787	0.049	520.380	520.241	0.027	353.720	353.448	0.077
10	671.910	671.741	0.025	629.620	629.774	0.024	434.090	433.720	0.085

A peculiar aspect of the curves is the sensitivity that each one exhibits with respect to the particular stiffness K_a, K_t and K_r. Between the lowest and the highest frequency values, a transit range exists. Its slope represents the notch sensitivity for that particular mode: for example, it appears that the axial stiffness variation involves the highest sensitivity. Therefore, it is possible to deduce that the notch sensitivity to the axial stiffness is higher than

the other stiffnesses, which agrees with the mechanical behaviour of arches.

Table 6 reports the beginning and the ending frequency values for the first 10 modes for each of the three plots, corresponding to $K_t = K_r = \infty$, $K_a = K_r = \infty$ and $K_a = K_t = \infty$. It is worth noting that the axial spring has the largest effect on the variation of the vibrating frequencies (Fig. 6).

However, from Table 6 is can be seen that when the variation of K_r is taken into account, the variation of the rotational elastic hinge does not influence the odd frequencies due to the particular location of the notch (key-section). This can be seen in Fig. 7, which shows the first six normal shapes for variation of the rotational stiffness K_r only. It is worth noting that the odd normal shapes 1, 3 and 5 are not affected by the stiffness variation of the elastic hinge.

In the end, the case of a Hinged-Clamped multi-stepped and multi-damaged parabolic arch (Fig. 8) is presented. The variation of the cross-sectional thickness is defined by the parameter $a = 0.010$ m, while the other dimension is $b = 0.045$m. Four arches are examined: a pristine one and three damaged cases with an increasing number of notched sections. It is worth noting that the frequency for each mode decreases monotonically when the number of notches increases. Numerical results are presented in table 7. Material properties are the same as those presented in table 2 and $\vartheta_{tot} = 120^\circ$. Fig. 9 shows the superimposition of the first normal shape for the four considered cases.

Finally, for the sake of completeness, it is important to point out that the GDQE method, as opposed to FE method, does not require any mesh refinement in the proximity of the damage in order to obtain accurate solutions.

7 Final remarks and conclusions

In this paper, an analytical formulation for modelling the dynamic behaviour of multi-stepped and multi-damaged parabolic arches has been presented. The coupled differential equations of motion for the generic arch segment, in terms of normal displacement, tangential displacement and rotation have been established according to the Hamilton's principle. All the effects related to axial, shearing and bending deformations are taken into account in the motion equations, as well as in the damage modelling. The numerical results for undamaged and damaged structural configurations have been calculated using the GDQ method for several combinations of boundary conditions.

Various combinations of parabolic arch segments and different notches are considered to investigate the influence of the structural parameters on the response of the system, in terms of the natural frequencies and mode shapes.

It should be noted that convergence and stability characteristics of the GDQ procedure are not explicitly investigated in this study, since the convergence rate of the natural frequencies is very fast and the stability of the numerical procedure is very good, as shown for circular arches by [69] and [21]. As a matter of fact, very accurate results can be obtained by using merely a few grid points. This aspect can be observed in the papers [70, 71].

With respect to the previously mentioned papers by the first author, the present study presents two main new findings concerning the form of the structure and the damage modelling. Regarding the shape of the structure, the parabolic arch model under investigation is a generalization of the circular one, which is characterized by a constant radius of curvature. In the case of a parabolic arch, the curvature radius has to be defined for each point of its axis, which can be represented by a general regular plane curve. The graphic representation of the curvature radius definition for each point is shown in Appendix A and the osculating circle at a point of the parabolic arch is involved, too.

As far as damage modelling is concerned, three elastic hinges represent the generalized elastic displacements of localized structural damage. These displacements correspond to the three parameters of movement of the kinematic arch model. It is noted that the foregoing papers of the first author, as well as papers of other authors, take only the rotational kinematic parameter into account. When the damaged parabolic arch is reduced to a circular one, and only the elastic rotational stiffness is modelled in evaluating the frequencies and mode shapes, the previously published results are obtained.

The local damage can be considered as a local stiffness reduction, represented by a combination of axial, normal and rotational elastic springs, that changes the dynamic behaviour of the structure. As mentioned before, much effort has been devoted to deal with the in-plane free vibration analysis of circular undamaged and circular damaged arch structures, but no one so far has investigated the parabolic multi-damaged arch.

Finally, two remarks can be made in relation to the damage modelling in arch structures. 1) The accuracy of equations (19), used for estimating the stiffness values of axial, normal and rotational springs, depends on the as-

Table 6: First ten natural frequencies for the limiting values of the spring stiffnesses ($K_a = 0, \infty$; $K_t = 0, \infty$ and $K_r = 0, \infty$): Straus7 - GDQ comparison.

Mode number	Straus7 [Hz]	GDQ [Hz]	Straus7 [Hz]	GDQ [Hz]	
	$K_a = 0$		$K_a = \infty$		Stiffnesses
1	12.157	12.172	25.301	25.339	
2	25,301	25.339	58.314	58.386	
3	61,246	61.358	101.184	101.333	
4	101,184	101.333	152.576	152.806	$K_t = \infty$,
5	157,034	157.317	216.238	216.635	$K_r = \infty$
6	216,238	216.635	290.276	290.902	
7	290,978	291.634	374.591	375.484	
8	374,591	375.484	468.134	469.347	
9	470,323	471.581	572.944	574.703	
10	572,944	574.703	672.339	673.087	
	$K_t = 0$		$K_t = \infty$		Stiffnesses
1	7,706	7.715	25.301	25.339	
2	44,186	44.267	58.314	58.386	
3	58,314	58.385	101.184	101.333	
4	129,471	129.699	152.576	152.806	$K_a = \infty$,
5	152,576	152.806	216.238	216.635	$K_r = \infty$
6	254,255	254.814	290.276	290.902	
7	290,276	290.902	374.591	375.484	
8	422,524	423.620	468.134	469.347	
9	468,134	469.346	572.944	574.703	
10	630,148	632.508	672.339	673.087	
	$K_r = 0$		$K_r = \infty$		Stiffnesses
1	25,301	25.339	25.301	25.339	
2	43,245	43.303	58.314	58.386	
3	101,184	101.333	101.184	101.333	
4	127,832	128.033	152.576	152.806	$K_a = \infty$,
5	216,238	216.635	216.238	216.635	$K_t = \infty$
6	254,254	254.812	290.276	290.902	
7	374,591	375.484	374.591	375.484	
8	422,041	423.127	468.134	469.347	
9	572,944	574.703	572.944	574.703	
10	627,704	629.999	672.339	673.087	

sumed extension s of the damage. Actually, the longitudinal extension of the damage s should be considered as an additional unknown parameter to be determined by a comparison between experimental and analytical data. 2) Moreover, when a notch is located at a section in which a stiffness jump occurs, the damage must be considered as belonging to the part of the parabolic arch with reduced dimensions of the cross section.

A deep and exhaustive investigation on the physical and mechanical motivation of the assumption at issue will be presented in a future paper by the authors.

List of main symbols

$f(\vartheta)$ = generic function;
α_{ij}^{n} = weighting coefficient;
$\mathcal{N}^{(e)}$ = total number of sampling points for the $e-th$ element;
n_e = total number of elements;
p_k = Lagrange interpolating polynomial;
$\mathcal{L}$ = Lagrange operator;
ϑ = intersection angle between the normal to the parabola and the auxiliary axis of the parabola;
$A(\vartheta)$ = cross-sectional area of the parabolic arch;
$I(\vartheta)$ = moment of inertia of the parabolic arch;
$R(\vartheta)$ = radius of curvature of the parabolic arch;
ϑ_{tot} = total angular width of the parabolic arch;
$u(\vartheta, t)$ = tangential displacement;
$v(\vartheta, t)$ = normal displacement;
$\varphi(\vartheta, t)$ = rotation angle of the arch cross-section;
$\varepsilon(\vartheta, t)$ = normal strain component;
$\gamma(\vartheta, t)$ = shear strain component;
$\kappa(\vartheta, t)$ = curvature;

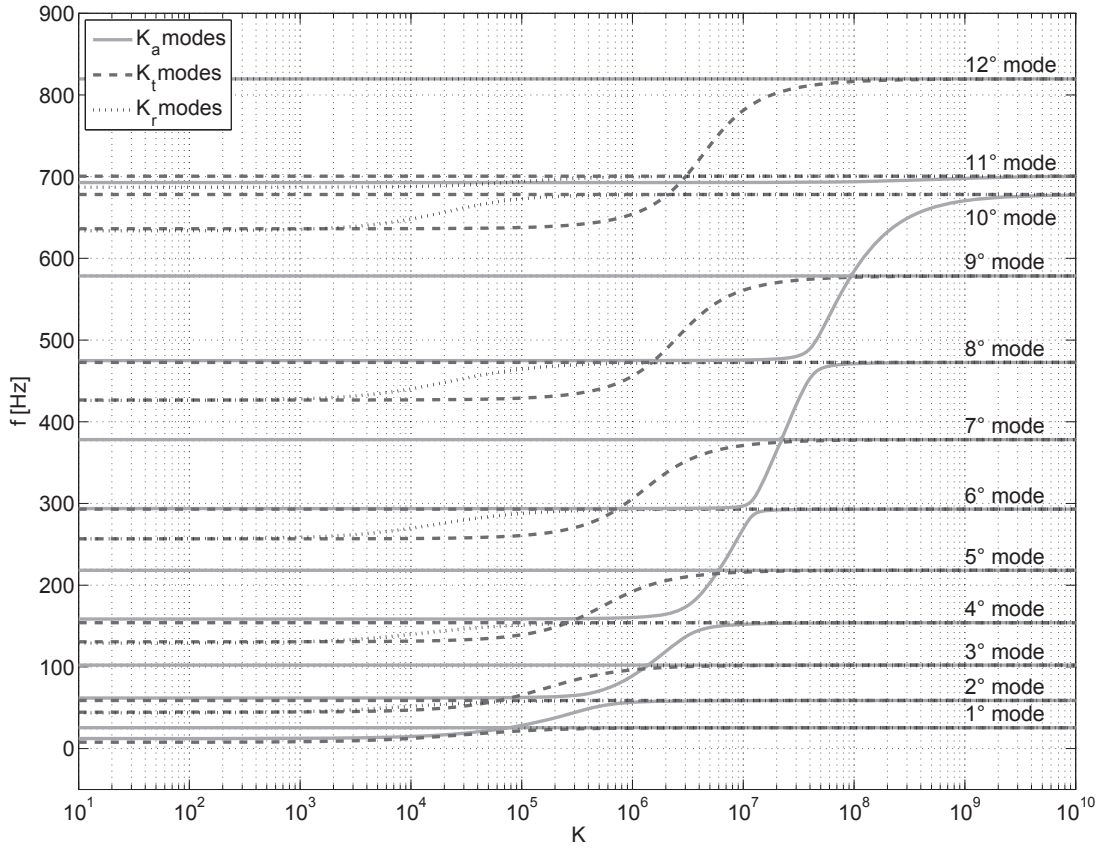

Figure 6: Effect of the variation of the single rigidity: K_a, K_t or K_r on the first 12 vibration modes of the damaged parabolic arch. The notch is located in the key section.

Table 7: First ten natural frequencies of three-stepped and multi-damaged Clamped-Hinged parabolic arches, only taking the rotational stiffness into account ($K_r = 219$kNm).

Mode number	Frequencies [Hz]			
	Position of notches along the arch			
	No notch	One notch at:	Two notches at:	Three notches at:
	/	$\vartheta_{notch} = 0.3\vartheta_{tot}$	$\vartheta_{notch} = \begin{cases} 0.3\vartheta_{tot} \\ 0.5\vartheta_{tot} \end{cases}$	$\vartheta_{notch} = \begin{cases} 0.3\vartheta_{tot} \\ 0.5\vartheta_{tot} \\ 0.7\vartheta_{tot} \end{cases}$
1	16.278	16.095	15.994	15.975
2	33.622	33.582	33.561	33.475
3	73.761	73.058	72.109	71.947
4	100.179	98.866	98.758	98.595
5	160.025	159.911	157.679	157.200
6	205.616	202.126	200.099	199.911
7	275.639	275.292	272.009	271.221
8	343.596	342.014	332.783	332.543
9	423.839	420.925	419.331	418.128
10	508.171	507.522	488.409	487.949

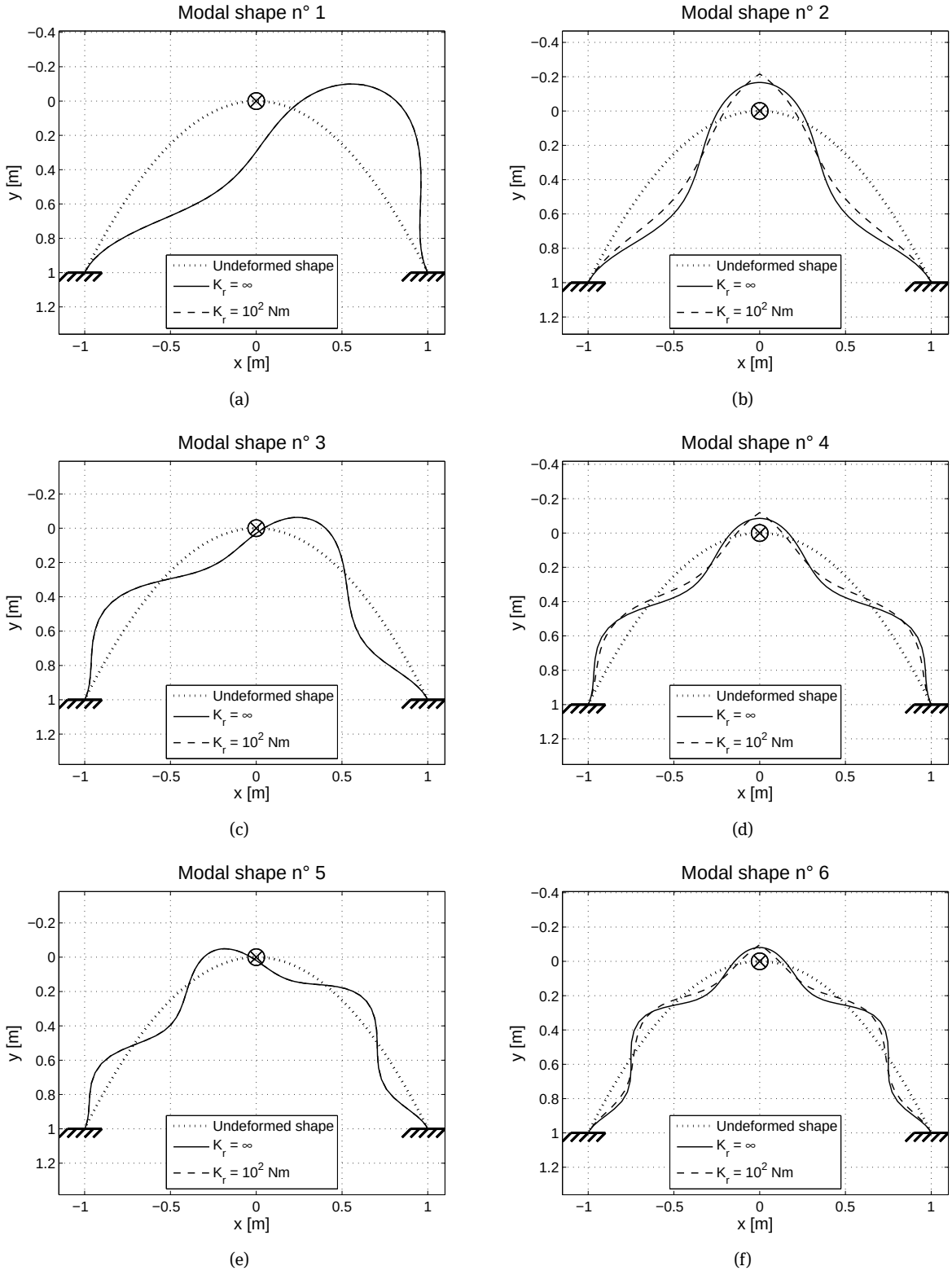

Figure 7: First six normal shapes of the parabolic arch, characterized by the two values of the rotational stiffness: $K_r = \infty$ and $K_r = 10^2$ Nm, with the discontinuity located in the key section.

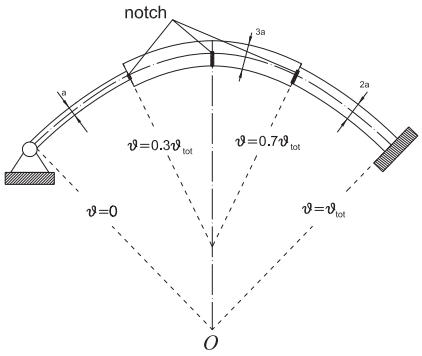

Figure 8: Schematic representation of a Hinged-Clamped three-stepped and multi-damaged parabolic arch.

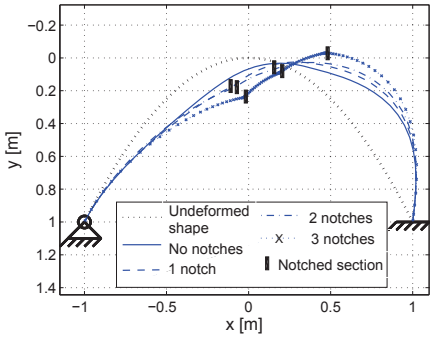

Figure 9: First modal shapes for Hinged-Clamped parabolic arches in different damage configurations.

$\delta\Pi$ = variation of the total potential energy;
δU = variation of the strain energy;
δT = variation of the kinetic energy;
δW_e = variation of the work of external forces;
$\boldsymbol{\varepsilon}$ = strain vector;
E = Young's modulus;
G = shear modulus;
ν = Poisson's ratio;
χ = shear factor;
Λ = shear area;
ρ = mass density;
$\mathbf{f}$ = vector of external forces;
$\mathbf{u}$ = generalized displacements vector;
$N(\vartheta, t)$ = axial force;
$T(\vartheta, t)$ = shear force;
$M(\vartheta, t)$ = bending moment;
K_a = axial elastic stiffness;
K_t = normal elastic stiffness;
K_r = rotational elastic stiffness;
A^D = area of the notched cross-section;
Λ^D = shear area of the notched cross-section;
I^D = moment of inertia of the notched cross-section;
s_{dam} = notch length;
R^{obs} = curvature radius of the osculating circle in the damage middle-point;
$\Delta\vartheta$ = opening angle of the notch;
$U^{(e)}$, $V^{(e)}$, $\Phi^{(e)}$ = vibration spatial amplitude values;
ω = frequency;
b = width of the cross-section;
h = height of the cross-section;
OXY = global reference system;
Pxy = local reference system.

Acknowledgement: The present investigation is one of the research topics treated by the Centre of Study and Research for the Identification of Materials and Structures (CIMEST) - "M. Capurso" of the Alma Mater Studiorum University of Bologna (Italy).

A Curvature radius for a regular curve of equation $y = f(x)$

In this appendix details of the implementation code are pointed out (Fig. A1). Generally speaking, the geometrical shape of a parabola is defined within three conditions. For sake of simplicity, the considered parabola (continuous line) is characterized by points A and B, and the vertex V is set in the origin of the coordinate system. The parabola equation is:

$$y = ax^2 \tag{A1}$$

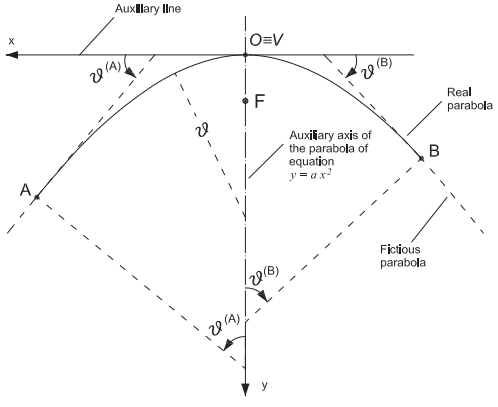

Figure A1: Parabolic arch referred to a global reference system.

The parabola is represented by the following parametric equations:

$$x = \frac{\tan\vartheta}{2a}, \qquad y = \frac{\tan^2\vartheta}{4a} \tag{A2}$$

where a is a parameter defined with respect to the focal distance $f = \frac{1}{4a}$ (if x_A and y_A are the input coordinates of the first extreme A of the parabola, a results to be $a = \frac{y_A}{x_A^2}$) and ϑ is the intersection angle of the normal at any point of the parabola and the symmetry axis. ϑ is positive (if the auxiliary axis rotates clockwise superimposing to the normal) or negative (if the auxiliary axis rotates anticlockwise superimposing to the normal). According to the definition can be $\vartheta_{tot} = |\vartheta_A| + |\vartheta_B|$.

B Mathematical steps

Let us assume the following relations connecting the internal forces $N^{(e)}(\vartheta, t)$, $T^{(e)}(\vartheta, t)$ and $M^{(e)}(\vartheta, t)$, and the displacements $u^{(e)}(\vartheta, t)$, $v^{(e)}(\vartheta, t)$ and $\varphi^{(e)}(\vartheta, t)$:

$$\begin{aligned}
N^{(e)}(\vartheta, t) &= \frac{EA^{(e)}}{R^{(e)}(\vartheta)}\left(\frac{\partial u^{(e)}(\vartheta, t)}{\partial\vartheta} - v^{(e)}(\vartheta, t)\right)\\
T^{(e)}(\vartheta, t) &= \frac{G\Lambda^{(e)}}{R^{(e)}(\vartheta)}\left(u^{(e)}(\vartheta, t) + \frac{\partial v^{(e)}(\vartheta, t)}{\partial\vartheta} + R^{(e)}(\vartheta)\,\varphi^{(e)}(\vartheta, t)\right)\\
M^{(e)}(\vartheta, t) &= \frac{EI^{(e)}}{R^{(e)}(\vartheta)}\frac{\partial\varphi^{(e)}(\vartheta, t)}{\partial\vartheta}
\end{aligned} \tag{A3}$$

The constitutive equations (A3) include the relationships between the strain components and the displacements components (6) for the $e-th$ segment of the arch. Using eqs. (A3), the equations of motion (13) can be re-written in the form:

$$\begin{aligned}
&\frac{1}{R^{(e)}(\vartheta)}\frac{\partial N^{(e)}(\vartheta, t)}{\partial\vartheta} - \frac{T^{(e)}(\vartheta, t)}{R^{(e)}(\vartheta)} + f^{(e)}(\vartheta, t) = \rho A^{(e)}\frac{\partial^2 u^{(e)}(\vartheta, t)}{\partial t^2}\\
&\frac{1}{R^{(e)}(\vartheta)}\frac{\partial T^{(e)}(\vartheta, t)}{\partial\vartheta} + \frac{N^{(e)}(\vartheta, t)}{R^{(e)}(\vartheta)} + q^{(e)}(\vartheta, t) = \rho A^{(e)}\frac{\partial^2 v^{(e)}(\vartheta, t)}{\partial t^2}\\
&\frac{1}{R^{(e)}(\vartheta)}\frac{\partial M^{(e)}(\vartheta, t)}{\partial\vartheta} - T^{(e)}(\vartheta, t) + m^{(e)}(\vartheta, t) = \rho I^{(e)}\frac{\partial^2\varphi^{(e)}(\vartheta, t)}{\partial t^2}
\end{aligned} \tag{A4}$$

It is worth noting that (A4) is a system of three partial differential equations that governs the small vibrations of parabolic stepped arches. Coupling takes place between the tangential displacement $u^{(e)}(\vartheta, t)$, normal displacement $v^{(e)}(\vartheta, t)$ and rotation $\varphi^{(e)}(\vartheta, t)$.

For the sake of completeness the differential system obtained by the substitution of eqs. (21) into (13) with the external forces vector equal to zero is shown in the following equations:

$$\begin{aligned}
&\left[\frac{EA^{(e)}}{\left[R^{(e)}\right]^2}\frac{\mathrm{d}^2}{\mathrm{d}\vartheta^2}+\left(\frac{E}{\left[R^{(e)}\right]^2}\frac{\mathrm{d}A^{(e)}}{\mathrm{d}\vartheta}-\frac{EA^{(e)}}{\left[R^{(e)}\right]^3}\frac{\mathrm{d}R^{(e)}}{\mathrm{d}\vartheta}\right)\frac{\mathrm{d}}{\mathrm{d}\vartheta}-\frac{G\Lambda^{(e)}}{\left[R^{(e)}\right]^2}\right]U^{(e)}+\\
&-\left[\left(\frac{EA^{(e)}}{\left[R^{(e)}\right]^2}+\frac{G\Lambda^{(e)}}{\left[R^{(e)}\right]^2}\right)\frac{\mathrm{d}}{\mathrm{d}\vartheta}+\left(\frac{E}{\left[R^{(e)}\right]^2}\frac{\mathrm{d}A^{(e)}}{\mathrm{d}\vartheta}-\frac{EA^{(e)}}{R^3}\frac{\mathrm{d}R^{(e)}}{\mathrm{d}\vartheta}\right)\right]V^{(e)}-\frac{G\Lambda^{(e)}}{\left[R^{(e)}\right]}\Phi^{(e)}=-\omega^2\rho A^{(e)}U^{(e)}
\end{aligned}$$

$$\begin{aligned}
&\left[\left(\frac{EA^{(e)}}{\left[R^{(e)}\right]^2}+\frac{G\Lambda^{(e)}}{\left[R^{(e)}\right]^2}\right)\frac{\mathrm{d}}{\mathrm{d}\vartheta}+\left(\frac{G}{\left[R^{(e)}\right]^2}\frac{\mathrm{d}\Lambda^{(e)}}{\mathrm{d}\vartheta}-\frac{G\Lambda^{(e)}}{\left[R^{(e)}\right]^3}\frac{\mathrm{d}}{\mathrm{d}\vartheta}\right)\right]U^{(e)}+\\
&+\left[\frac{G\Lambda^{(e)}}{\left[R^{(e)}\right]^2}\frac{\mathrm{d}^2}{\mathrm{d}\vartheta^2}+\left(\frac{G}{\left[R^{(e)}\right]^2}\frac{\mathrm{d}\Lambda^{(e)}}{\mathrm{d}\vartheta}-\frac{G\Lambda^{(e)}}{\left[R^{(e)}\right]^3}\frac{\mathrm{d}R^{(e)}}{\mathrm{d}\vartheta}\right)\frac{\mathrm{d}}{\mathrm{d}\vartheta}-\frac{EA^{(e)}}{\left[R^{(e)}\right]^2}\right]V^{(e)}+\\
&+\left[\frac{G\Lambda^{(e)}}{\left[R^{(e)}\right]}\frac{\mathrm{d}}{\mathrm{d}\vartheta}+\frac{G}{\left[R^{(e)}\right]}\frac{\mathrm{d}\Lambda^{(e)}}{\mathrm{d}\vartheta}\right]\Phi^{(e)}=-\omega^2\rho A^{(e)}V^{(e)}
\end{aligned}\tag{A5}$$

$$\begin{aligned}
&\left[-\frac{G\Lambda^{(e)}}{\left[R^{(e)}\right]}\right]U^{(e)}-\left[\frac{G\Lambda^{(e)}}{\left[R^{(e)}\right]}\frac{\mathrm{d}}{\mathrm{d}\vartheta}\right]V^{(e)}+\\
&+\left[\frac{EI^{(e)}}{\left[R^{(e)}\right]^2}\frac{\mathrm{d}^2}{\mathrm{d}\vartheta^2}+\left(\frac{E}{\left[R^{(e)}\right]^2}\frac{\mathrm{d}I^{(e)}}{\mathrm{d}\vartheta}-\frac{EI^{(e)}}{\left[R^{(e)}\right]^3}\frac{\mathrm{d}R^{(e)}}{\mathrm{d}\vartheta}\right)\frac{\mathrm{d}}{\mathrm{d}\vartheta}-G\Lambda^{(e)}\right]\Phi^{(e)}=-\omega^2\rho I^{(e)}\Phi^{(e)}
\end{aligned}$$

The boundary conditions for the Clamped-Clamped arch, imposed at the extremes of the arch assume the form:

$$\begin{aligned}
&U^{(1)}(0)=0, \qquad U^{(n_e)}(\vartheta_{tot})=0,\\
&V^{(1)}(0)=0, \qquad V^{(n_e)}(\vartheta_{tot})=0,\\
&\Phi^{(1)}(0)=0, \qquad \Phi^{(n_e)}(\vartheta_{tot})=0
\end{aligned}\tag{A6}$$

For the Hinged-Hinged arch one gets:

$$\begin{aligned}
&U^{(1)}(0)=0, \qquad U^{(n_e)}(\vartheta_{tot})=0,\\
&V^{(1)}(0)=0, \qquad V^{(n_e)}(\vartheta_{tot})=0,\\
&\frac{\mathrm{d}\Phi^{(1)}(0)}{\mathrm{d}\vartheta}=0, \qquad \frac{\mathrm{d}\Phi^{(n_e)}(\vartheta_{tot})}{\mathrm{d}\vartheta}=0
\end{aligned}\tag{A7}$$

and for the Clamped-Free arch the following results are obtained:

$$\begin{aligned}
&U^{(1)}(0)=0, \quad \frac{\mathrm{d}U^{(n_e)}(\vartheta_{tot})}{\mathrm{d}\vartheta}-V^{(n_e)}(\vartheta_{tot})=0,\\
&V^{(1)}(0)=0, \quad U^{(n_e)}(\vartheta_{tot})+\frac{\mathrm{d}V^{(n_e)}(\vartheta_{tot})}{\mathrm{d}\vartheta}+R^{(n_e)}\Phi^{(n_e)}(\vartheta_{tot})=0,\\
&\Phi^{(1)}(0)=0, \quad \frac{\mathrm{d}\Phi^{(n_e)}(\vartheta_{tot})}{\mathrm{d}\vartheta}=0
\end{aligned}\tag{A8}$$

Furthermore, the continuity and the equilibrium conditions between the $e-th$ and the $(e+1)-th$ arch segments at a generic ϑ require that:

$$\begin{aligned} U^{(e+1)}(\vartheta) &= U^{(e)}(\vartheta), \\ V^{(e+1)}(\vartheta) &= V^{(e)}(\vartheta), \\ \Phi^{(e+1)}(\vartheta) &= \Phi^{(e)}(\vartheta), \\ N^{(e+1)}(\vartheta) &= N^{(e)}(\vartheta), \\ T^{(e+1)}(\vartheta) &= T^{(e)}(\vartheta), \\ M^{(e+1)}(\vartheta) &= M^{(e)}(\vartheta) \end{aligned} \tag{A9}$$

for $e = 1, \cdots, n_e - 1$. Considering the presence of a notch, the continuity conditions (20) take the following form:

$$\begin{aligned} K_a \left[U^{(e+1)}(\vartheta) - U^{(e)}(\vartheta) \right] &= N^{(e)}(\vartheta), \\ K_t \left[V^{(e+1)}(\vartheta) - V^{(e)}(\vartheta) \right] &= T^{(e)}(\vartheta), \\ K_r \left[\Phi^{(e+1)}(\vartheta) - \Phi^{(e)}(\vartheta) \right] &= M^{(e)}(\vartheta), \\ N^{(e+1)}(\vartheta) &= N^{(e)}(\vartheta), \\ T^{(e+1)}(\vartheta) &= T^{(e)}(\vartheta), \\ M^{(e+1)}(\vartheta) &= M^{(e)}(\vartheta) \end{aligned} \tag{A10}$$

References

[1] G. Karami, P. Malekzadeh, In-plane free vibration analysis of circular arches with varying cross-sections using differential quadrature method, Journal of Sound and Vibration 274 (3–5) (2004) 777 – 799.

[2] J.-S. Wu, L.-K. Chiang, A new approach for free vibration analysis of arches with effects of shear deformation and rotary inertia considered, Journal of Sound and Vibration 277 (1–2) (2004) 49 – 71.

[3] E. Viola, E. Artioli, M. Dilena, Analytical and differential quadrature results for vibration analysis of damaged circular arches, Journal of Sound and Vibration 288 (4–5) (2005) 887 – 906.

[4] M. N. Cerri, G. C. Ruta, Detection of localised damage in plane circular arches by frequency data, Journal of Sound and Vibration 270 (1–2) (2004) 39 – 59.

[5] M.-S. Marefat, E. Ghahremani-Gargary, S. Ataei, Load test of a plain concrete arch railway bridge of 20-m span, Construction and Building Materials 18 (9) (2004) 661 – 667.

[6] K.-H. Ng, C. A. Fairfield, Modifying the mechanism method of masonry arch bridge analysis, Construction and Building Materials 18 (2) (2004) 91 – 97.

[7] M. N. Cerri, M. Dilena, G. C. Ruta, Vibration and damage detection in undamaged and cracked circular arches: Experimental and analytical results, Journal of Sound and Vibration 314 (1–2) (2008) 83 – 94.

[8] G. de Felice, Assessment of the load-carrying capacity of multi-span masonry arch bridges using fibre beam elements, Engineering Structures 31 (8) (2009) 1634 – 1647.

[9] K. M. Ahmed, Free vibration of curved sandwich beams by the method of finite elements, Journal of Sound and Vibration 18 (1) (1971) 61 – 74.

[10] D. G. Ashwell, A. B. Sabir, T. M. Roberts, Further studies in the application of curved finite elements to circular arches, International Journal of Mechanical Sciences 13 (6) (1971) 507 – 517.

[11] M. Petyt, C. C. Fleischer, Free vibration of a curved beam, Journal of Sound and Vibration 18 (1) (1971) 17 – 30.

[12] D. J. Dawe, Curved finite elements for the analysis of shallow and deep arches, Computers and Structures 4 (3) (1974) 559 – 580.

[13] D. J. Dawe, Numerical studies using circular arch finite elements, Computers and Structures 4 (4) (1974) 729 – 740.

[14] G. Prathap, The curved beam/deep arch/finite ring element revisited, International Journal for Numerical Methods in Engineering 21 (3) (1985) 389–407.

[15] J. K. Choi, J. K. Lim, General curved beam elements based on the assumed strain fields, Computers and Structures 55 (3) (1995) 379 – 386.

[16] E. Viola, E. Artioli, The g.d.q. method for the harmonic dynamic analysis of rotational shell structural elements, Structural Engineering and Mechanics 17 (6) (2004) 789–817.

[17] E. Artioli, P. L. Gould, E. Viola, A differential quadrature method solution for shear deformable shells of revolution, Engineering Structures 27 (2005) 1879–1892.

[18] E. Artioli, E. Viola, Static analysis of shear-deformable shells of revolution via g.d.q. method, Structural Engineering and Mechanics 19 (4) (2005) 459–475.

[19] F. Tornabene, N. Fantuzzi, F. Ubertini, E. Viola, Strong formulation finite element method based on differential quadrature: a survey, Applied Mechanics Reviews doi:10.1115/1.4028859, In Press.

[20] A. Pau, A. Greco, F. Vestroni, Numerical and experimental detection of concentrated damage in a parabolic arch by measured frequency variations, Journal of Vibration and Control 17 (4) (2010) 605–614.

[21] E. Viola, M. Dilena, F. Tornabene, Analytical and numerical results for vibration analysis of multi-stepped and multi-damaged circular arches, Journal of Sound and Vibration 299 (1-2) (2007) 143 – 163.

[22] B. D. Reddy, M. B. Volpi, Mixed finite element methods for the circular arch problem, Computer Methods in Applied Mechanics and Engineering 97 (1) (1992) 125 – 145.

[23] P. Ricci, E. Viola, Stress intensity factors for cracked t-sections and dynamic behaviour of t-beams, Engineering Fracture Mechanics 73 (1) (2006) 91 – 111.

[24] R. Bellman, J. Casti, Differential quadrature and long-term integration, Journal of Mathematical Analysis and Applications 34 (2) (1971) 235 – 238.

[25] R. Bellman, B. G. Kashef, J. Casti, Differential quadrature: A technique for the rapid solution of nonlinear partial differential equations, Journal of Computational Physics 10 (1) (1972) 40 – 52.

[26] F. Civan, C. M. Sliepcevich, Differential quadrature for multi-dimensional problems, Journal of Mathematical Analysis and Applications 101 (2) (1984) 423 – 443.

[27] K. J. Kang, C. W. Bert, A. G. Striz, Vibration analysis of shear deformable circular arches by the differential quadrature method,

Journal of Sound and Vibration 181 (2) (1995) 353 – 360.
[28] C. W. Bert, M. Malik, Differential quadrature method in computational mechanics: A review, Applied Mechanics Reviews 49 (1) (1996) 1–28.
[29] K. J. Kang, C. W. Bert, A. G. Striz, Vibration and buckling analysis of circular arches using dqm, Computers and Structures 60 (1) (1996) 49 – 57.
[30] C.-N. Chen, A generalized differential quadrature element method, Computer Methods in Applied Mechanics and Engineering 188 (1–3) (2000) 553 – 566.
[31] G. R. Liu, T. Y. Wu, In-plane vibration analyses of circular arches by the generalized differential quadrature rule, International Journal of Mechanical Sciences 43 (11) (2001) 2597 – 2611.
[32] T. Y. Wu, G. R. Liu, Y. Y. Wang, Application of the generalized differential quadrature rule to initial-boundary-value problems, Journal of Sound and Vibration 264 (4) (2003) 883 – 891.
[33] C. Shu, Differential quadrature and its application in engineering, Springer, 2000.
[34] E. Viola, F. Tornabene, Vibration analysis of conical shell structures using GDQ method, Far East Journal of Applied Mathematics 25 (1) (2006) 23–39.
[35] A. Marzani, F. Tornabene, E. Viola, Nonconservative stability problems via generalized differential quadrature method, Journal of Sound and Vibration 315 (1-2) (2008) 176–196.
[36] F. Tornabene, E. Viola, Free vibration analysis of functionally graded panels and shells of revolution, Meccanica 44 (3) (2009) 255–281.
[37] E. Viola, F. Tornabene, Free vibrations of three parameter functionally graded parabolic panels of revolution, Mechanics Research Communications 36 (5) (2009) 587–594.
[38] E. Viola, F. Tornabene, N. Fantuzzi, Generalized differential quadrature finite element method for cracked composite structures of arbitrary shape, Composite Structures 106 (1) (2013) 815–834.
[39] E. Viola, F. Tornabene, E. Ferretti, N. Fantuzzi, On static analysis of composite plane state structures via GDQFEM and cell method, CMES 94 (5) (2013) 421–458.
[40] N. Fantuzzi, F. Tornabene, E. Viola, A. J. M. Ferreira, A strong formulation finite element method (sfem) based on RBF and GDQ techniques for the static and dynamic analyses of laminated plates of arbitrary shape, Meccanica 49 (1) (2014) 2503–2542.
[41] M. Kisa, Vibration and stability of axially loaded cracked beams, Structural Engineering and Mechanics 44 (2012) 305–323.
[42] M. Kisa, J. A. Brandom, Free vibration analysis of multiply open-edge cracked beams by component mode synthesis, Structural Engineering and Mechanics 10 (2000) 81–92.
[43] N. Fallah, M. Mousavi, An inverse approach for the calculation of flexibility coefficient of open-side cracks in beam type structures, Structural Engineering and Mechanics 41 (2012) 285–297.
[44] H. R. Öz, In-plane vibration of cracked slightly curved beams, Structural Engineering and Mechanics 36 (2010) 679–695.
[45] E. Viola, A. Marzani, Crack effect on dynamic stability of beams under conservative and nonconservative forces, Engineering Fracture Mechanics 71 (2004) 699–718.
[46] A. Marzani, E. Viola, Effect of boundary conditions on the stability of beams under conservative and non-conservative forces, Structural Engineering and Mechanics 16 (2003) 195–217.
[47] Z. Cao, Y. Liu, A new numerical modelling for evaluating the stress intensity factors in 3-d fracture, Structural Engineering and Mechanics 43 (2012) 321–336.
[48] M. R. Ayatollahi, R. Hashemi, H. Rokhi, New formulation for vibration analysis of timoshenko beam with double-sided cracks, Structural Engineering and Mechanics 34 (2010) 475–490.
[49] Z. Y. He, Z. R. Lu, Time domain identification of multiply cracks in a beam, Structural Engineering and Mechanics 35 (2010) 773–789.
[50] H. Y. Gao, X. L. Guo, X. F. Hu, Crack identification based on kriging surrogate model, Structural Engineering and Mechanics 41 (2012) 25–41.
[51] A. Greco, A. Pau, Detection of a concentrated damage in a parabolic arch by measured static displacements, Structural Engineering and Mechanics 39 (2011) 751–765.
[52] A. H. Gandomi, M. G. Sahab, A. Rahai, A dynamic non-destructive damage detection methodology for orthotropic plate structures, Structural Engineering and Mechanics 39 (2011) 223–239.
[53] E. Viola, P. Bocchini, Non-destructive parametric system identification and damage detection in truss structures by static tests, Structure and Infrastructure Engineering: Maintenance, Management, Life-Cycle Design and Performance 9 (2013) 384–402.
[54] F. Civan, C. M. Sliepcevich, Application of differential quadrature in solution of pool boiling in cavities, Proceedings of the Oklahoma Academy of Science 65 (1985) 73–78.
[55] E. Viola, F. Tornabene, E. Ferretti, N. Fantuzzi, Soft core plane state structures under static loads using GDQFEM and cell method, CMES 94 (4) (2013) 301–329.
[56] E. Viola, F. Tornabene, E. Ferretti, N. Fantuzzi, Gdqfem numerical simulations of continuous media with cracks and discontinuities, CMES 94 (4) (2013) 331–369.
[57] N. Fantuzzi, F. Tornabene, E. Viola, Generalized differential quadrature finite element method for vibration analysis of arbitrarily shaped membranes, International Journal of Mechanical Sciences 79 (1) (2014) 216–251.
[58] T. M. Tharp, A finite element for edge-cracked beam columns, International Journal for Numerical Methods in Engineering 24 (10) (1987) 1941–1950.
[59] E. Cabib, L. Freddi, A. Morassi, D. Percivale, Thin notched beams, Journal of elasticity 64 (2001) 157–178.
[60] E. Viola, L. Federici, L. Nobile, Detection of crack location using cracked beam element method for structural analysis, Theoretical and Applied Fracture Mechanics 36 (1) (2001) 23 – 35.
[61] E. Viola, L. Nobile, L. Federici, Formulation of cracked beam element for structural analysis, Journal of Engineering Mechanics 128 (2) (2002) 220–230.
[62] N. Fantuzzi, F. Tornabene, Strong formulation finite element method for arbitrarily shaped laminated plates - i. theoretical analysis, Advances in Aircraft and Spacecraft Science 1 (2) (2014) 125–143.
[63] N. Fantuzzi, F. Tornabene, Strong formulation finite element method for arbitrarily shaped laminated plates - ii. numerical analysis, Advances in Aircraft and Spacecraft Science 1 (2) (2014) 145–175.
[64] F. Tornabene, E. Viola, Vibration analysis of spherical structural elements using the GDQ method, Computers and Mathematics with Applications 53 (10) (2006) 1538–1560.
[65] F. Tornabene, E. Viola, 2-d solution for free vibrations of parabolic shells using generalized differential quadrature method, European Journal of Mechanics - A/Solids 27 (6) (2008) 1001–1025.

[66] F. Tornabene, E. Viola, D. J. Inman, 2-d differential quadrature solution for vibration analysis of functionally graded conical, cylindrical shell and annular plate structures, Journal of Sound and Vibration 328 (3) (2009) 259–290.

[67] F. Tornabene, A. Marzani, E. Viola, I. Elishakoff, Critical flow speeds of pipes conveying fluid by the generalized differential quadrature method, Advances in Theoretical and Applied Mechanics 3 (3) (2010) 121–138.

[68] E. Tufekci, O. Ozdemirci Yigit, Effects of geometric parameters on in-plane vibrations of two-stepped circular beams, Structural Engineering and Mechanics 42 (2) (2012) 131–152.

[69] E. Viola, F. Tornabene, Vibration analysis of damaged circular arches with varying cross-section, Struct. Int. Durab. (SID-SDHM) 1 (2) (2005) 155 – 169.

[70] E. Viola, F. Tornabene, Free vibrations of four-parameter functionally graded parabolic panels and shells of revolution, European Journal of Mechanics - A/Solids 28 (5) (2009) 991–1013.

[71] F. Tornabene, Free vibration analysis of functionally graded conical, cylindrical shell and annular plate structures with a four-parameter power-law distribution, Computer Methods in Applied Mechanics and Engineering 198 (37-40) (2009) 2911–2935.